PLOS ONE

RESEARCH ARTICLE

The bidirectional role of $GABA_A$ and $GABA_B$ receptors during the differentiation process of neural precursor cells of the subventricular zone

Nadia Estefanía Gutierrez-Castañeda[1], Vladimir Allex Martínez-Rojas[1], Lenin David Ochoa-de la Paz[2], Emilio J. Galván[1,3]*

1 Departamento de Farmacobiología, Centro de Investigación y de Estudios Avanzados del Instituto Politécnico Nacional, Ciudad de México, México, **2** Laboratorio de Neurobiología Molecular y Celular de la Glía, Unidad de Investigación UNAM-APEC, México City, México, **3** Centro de Investigación sobre el Envejecimiento, Ciudad de México, México

* ejgalvan@cinvestav.mx

Citation: Gutierrez-Castañeda NE, Martínez-Rojas VA, Ochoa-de la Paz LD, Galván EJ (2024) The bidirectional role of $GABA_A$ and $GABA_B$ receptors during the differentiation process of neural precursor cells of the subventricular zone. PLoS ONE 19(6): e0305853. https://doi.org/10.1371/journal.pone.0305853

Editor: Anju Vasudevan, Huntington Medical Research Institutes, UNITED STATES

Received: March 25, 2024

Accepted: June 5, 2024

Published: June 24, 2024

Data Availability Statement: data available: https://www.kaggle.com/datasets/nadiaestefana/the-bidirectional-role-of-gabaa-and-gabab/settings.

Funding: • PAPIIT-UNAM IN221823, Presupuesto Interno Facultad de Medicina (Id 49) (Financial and Material support). • Conacyht grant (783563) to NEGC (Financial support). • Cinvestav-IPN to EJG (Financial and Material support) • The funders had no role in study design, data collection and

Abstract

The intricate process of neuronal differentiation integrates multiple signals to induce transcriptional, morphological, and electrophysiological changes that reshape the properties of neural precursor cells during their maturation and migration process. An increasing number of neurotransmitters and biomolecules have been identified as molecular signals that trigger and guide this process. In this sense, taurine, a sulfur-containing, non-essential amino acid widely expressed in the mammal brain, modulates the neuronal differentiation process. In this study, we describe the effect of taurine acting via the ionotropic $GABA_A$ receptor and the metabotropic $GABA_B$ receptor on the neuronal differentiation and electrophysiological properties of precursor cells derived from the subventricular zone of the mouse brain. Taurine stimulates the number of neurites and favors the dendritic complexity of the neural precursor cells, accompanied by changes in the somatic input resistance and the strength of inward and outward membranal currents. At the pharmacological level, the blockade of $GABA_A$ receptors inhibits these effects, whereas the stimulation of $GABA_B$ receptors has no positive effects on the taurine-mediated differentiation process. Strikingly, the blockade of the $GABA_B$ receptor with CGP533737 stimulates neurite outgrowth, dendritic complexity, and membranal current kinetics of neural precursor cells. The effects of taurine on the differentiation process involve Ca^{2+} mobilization and the activation of intracellular signaling cascades since chelation of intracellular calcium with BAPTA-AM, and inhibition of the CaMKII, ERK1/2, and Src kinase inhibits the neurite outgrowth of neural precursor cells of the subventricular zone.

Introduction

Adult neurogenesis, the process by which newborn neurons integrate into consolidated neural circuits, has been extensively studied in the subgranular zone of the dentate gyrus and the

analysis, decision to publish, or preparation of the manuscript.

Competing interests: • The authors have declared that no competing interests exist.

subventricular zone (SVZ) of the lateral ventricles. Neurons stemming from the subgranular zone merge into the granule cell layer and develop a glutamatergic phenotype, contributing to hippocampal-related functions [1–4]. On the other hand, most of the SVZ-derived neurons undergo a rostral migration that culminates with their integration into the olfactory bulb. These newborn cells develop a GABAergic phenotype and are, indeed, interneurons [5, 6] whose function has been linked to accelerating the learning of olfactory discrimination and short-term olfactory memory [7, 8].

Morphologically, adult neurogenesis is accompanied by neurite outgrowth and the formation of a multifarious neurite branching rearrangement associated with neuronal maturation [9]. Neurite outgrowth is triggered by depolarizing events that favor transient increases in intracellular calcium and the activation of signaling cascades that promote neurite elongation and synapse formation [10]. Consistent with this tenet, neuronal precursor cells (NPCs) of the SVZ are stem cells endowed with multiple signaling cascades whose activation converges in the phosphorylation of the cAMP response element-binding protein (CREB), a transcription factor required for neurite outgrowth of NPCs [11, 12].

The signaling cascades involved in the differentiation process of NPCs are activated by diverse neurotransmitters, hormones, and biomolecules, including taurine, a free sulfur-amino acid found in high concentrations in the mammalian brain [13]. It has been well established that taurine has a neurotrophic effect on neurite outgrowth and the thickness of developing neurites [14]. In a recent study, we demonstrated that the development of neurite complexity of NPC SVZ mediated by taurine is accompanied by the functional expression of ion channels that reshape the passive electrophysiological properties of NPC SVZ and favor the appearance of active properties, including action potential generation and a Ca^{2+}-dependent afterhyperpolarization [15].

Interestingly, a series of studies have documented that NPCs also express $GABA_B$ receptors ($GABA_BR$). The blockade of $GABA_BR$ promotes hippocampal neurogenesis [16], and in neocortical-derived neurospheres, the blockade of $GABA_BR$ favors the proliferation and differentiation process [17]. Contrary to these findings, the pharmacological activation of $GABA_BR$ has been reported to suppress adult hippocampal neurogenesis [18, 19]. Despite the possible relevance of $GABA_BR$ in the differentiation process of NPCs, the expression of $GABA_BR$ on NPC SVZ and its role in the differentiation process of NPC SVZ remains unexplored.

To close this gap, in this study, we explored the interaction of taurine with GABA receptors in the maturation process of NPC SVZ. We first demonstrated the presence of $GABA_BR$ in neurospheres of NPC SVZ; then, we explored the role of taurine in the establishment of inward and outward membrane currents that shape the electrophysiological properties associated with neuronal maturation; and finally, we demonstrated the role of several intracellular signaling cascades in the neurite formation of NPC SVZ. Our findings demonstrate that the abundant neuroactive molecule taurine plays a significant role in the neurophysiological maturation of NPC SVZ via an antagonistic modulation of ionotropic and metabotropic GABA receptors acting in a nonsynaptic fashion.

Material and methods

Primary neural precursor cell culture

The experimental procedures were conducted in strict accordance with the Mexican Official Norm for the use and care of laboratory animals "NOM-062-ZOO-1999," the Guide for the Care and Use of Laboratory Animals of the National Institutes of Health, and with the approval of the Institutional Animal Care and Use Committee of the National University of Mexico (FMED/DI/068/2019, CICUAL018-CIC-2019). Eight-day-old CD1 mice were used to

obtain NPC SVZ. The mice were quickly sacrificed by decapitation, their brain was removed, and the SVZ was isolated. Then, the tissue was mechanically dissociated and placed in a DMEM/F12 medium (Dulbecco's Modified Eagle Medium/Nutrient Mixture F-12. Gibco; Thermo Fisher Scientific, Inc., Waltham, MA, USA) and centrifuged for 5 min at 1000 rpm. The supernatant was removed, and the pellet was resuspended and cultured in a growth medium (DMEM/F12 supplemented with B27, plus epidermal growth factor and fibroblast growth factor 2) to promote progenitor cell proliferation and SVZ neurosphere formation.

The resulting cultures were maintained at 37˚C and 5% CO_2. After seven days, the primary neurospheres were mechanically disaggregated with trypsin, and a trypsin inhibitor (1:1) was added to stop the reaction. The cells were then cultured in a growth medium for four to five days at 37˚C and 5% CO_2. For the differentiation process of NPC SVZ, disaggregated cells of the secondary SVZ neurospheres were cultured in 48 wells pretreated with poly-D-lysine (Sigma-Aldrich, St. Louis, MO, USA) and a differentiation medium (DMEM/F12 supplemented with 1% fetal bovine serum (FBS) and complemented with taurine (10 mM)). The taurine dose used in this study was previously determined by performing a dose-response curve [15].

To evaluate the role of the $GABA_A$ or $GABA_B$ receptor in the differentiation process, the cultured cells were preincubated for one hour with the $GABA_A$ receptor antagonist picrotoxin (100 μM), the $GABA_B$ receptor antagonist CGP55845 (5 μM), or the $GABA_B$ receptor agonist baclofen (100 μM). To determine the participation of different signaling cascades in the differentiation process induced by taurine through GABA receptors, the cells were cultured for differentiation for three days and preincubated with BAPTA-AM (100 μM) in a Krebs-Ringer Buffer without calcium for 30 min. Then, KN93 (10 μM), FR180204 (10 μM), and SrcI (1 μM) were co-incubated in the presence of taurine 10 (mM) for seven days. All the drugs were purchased from Sigma-Aldrich, St. Louis, MO, USA.

Immunofluorescence assay

The cultured cells were fixed with cold paraformaldehyde (4%), washed with phosphate-buffered saline (PBS) + 0.1% bovine serum albumin (BSA; 3 × 5 min), and permeabilized/blocked with PBS + 0.1% BSA + 10% FBS + 0.3% Triton X-100 for 1 h at room temperature. The cells were subsequently incubated overnight with the primary antibodies nestin (Cell Signaling Technology Cat# 4760, RRID: AB_2235913) [1:300]), KI67 (Cell Signaling Technology Cat# 9027, RRID:AB_2636984) [1:100), GABABR1(Santa Cruz Biotechnology Cat# sc-166408, RRID:AB_2108175), doublecortin (DCX, Abcam Cat# ab18723, RRID: AB_732011) [1:1000]), and MAP2 (Cell Signaling Technology Cat# 8707, RRID: AB_2722660). The primary antibodies were removed the following day, followed by a 1-h incubation with the secondary antibodies Alexa Fluor-488 anti-rabbit 9 and Alexa Fluor-647 anti-mouse. The excess secondary antibody was then washed and removed from the preparation assembly. The nuclei were stained with DAPI (20 μg/mL) included in the mounting solution (100/500 μL).

Quantitative analysis for cell markers

Microphotographs were obtained with the cell imaging multi-mode plate reader Cytation™ 5 (BioTek Instruments Inc., Winooski, VT, USA) using a green fluorescent protein (GFP) filter cube (excitation 469/35 nm; emission 525/39 nm; dichroic mirror 497 nm) and 465 nm LED; a Texas Red filter cube (excitation 586/15 nm; emission 647/67 nm; dichroic mirror 605 nm) and 590 nm LED; and a 4′,6-diamidino-2-phenylindole (DAPI) filter cube (excitation 377/50 nm; emission 447/60 nm; dichroic mirror 409) and 365 nm LED. Microphotographs of five fields were randomly selected from each coverslip, and the number of total (DAPI positive)

cells and cells positive for the different markers in the selected fields were quantified. Cell images were processed using Gen5™ software (BioTek Instruments Inc.). The results were expressed as the percentage of positive cells out of the total number of cells.

Morphometric analysis of dendritic arborization of DCX- and MAP2-positive cells

Microphotographs of DCX-positive (DCX+) cells were randomly obtained with a 20x magnification lens. DCX+ cells were analyzed for each experimental condition. The number of primary, secondary, and tertiary neurites and the length of the primary neurites were determined with Gen 5 3.04. The difference between primary, secondary, and tertiary neurites was analyzed in the different experimental conditions. Manual quantification of dendritic arborization was performed by counting the number of primary dendrites for each neuron using ImageJ software [20] with the Sholl analysis plug-in v3.4.2 [21]. Primary neurites were defined as those that originated directly from the soma; secondary and tertiary neurites were defined as those that originated from primary and secondary neurites, respectively. Researchers were blinded to experimental groups prior to performing all morphometric analyses.

Whole-cell patch-clamp recordings

Dissociated NPC SVZ from SVZ neurospheres were taken from a petri dish containing the cell culture, mounted on a coverslip, and transferred to a submersion recording chamber. They were visualized with infrared differential interference contrast optics coupled to a Nikon FN1 microscope (Nikon Corporation, Minato, Tokyo, Japan). The NPC-SVZ were continuously perfused with Ringer's solution at the rate of 3–4 mL/min^{-1} with the help of a peristaltic pump (120S, Watson-Marlow, Wilmington, MA, USA). The composition of the bath solution was as follows (mM): 132 NaCl, 3.6 KCl, 1.5 $MgCl_2$, 2.5 $CaCl_2$, 10 HEPES, and 10 D-glucose; pH = 7.30–7.40; osmolarity = 280–290 mOsm. The recording chamber temperature was maintained at 32 ± 1˚C with a single channel temperature controller (TC-324C, Warner Instruments, Hamden, CT, USA). The patch pipettes were pulled from borosilicate glasses using a micropipette puller (P97, Sutter Instruments, Novato, CA, USA). The puller was programmed to obtain pipettes with a tip resistance of 3–5 MΩ when filled with an intracellular solution containing the following (mM): 140 KCl, 1.1 EGTA, 10 HEPES, 3 Mg^{2+}-ATP, 0.3 Na^{+}-GTP, and pH = 7.20–7.30. Whole-cell recordings were performed with an Axopatch 200B amplifier (Molecular Devices, San José, CA, USA). Acquired data were digitized at a sampling frequency of 20 kHz and filtered at 2 kHz with a Digidata 1322A (Axon Instruments, Palo Alto, CA, USA). Signals were acquired and analyzed offline with pCLAMP 10.6 software (Molecular Devices).

Determination of intrinsic properties

The resting membrane potential (RMP) was determined after the initial membrane break-in from giga-seal to whole-cell configuration in voltage clamp mode. After 2–3 min. of stabilization, a series of negative and positive voltage commands from -100 to +50 (500 ms, 250 pA increments) were injected to determine the input resistance (R_N) and membrane time constant (τ_{memb}). The R_N was calculated as the slope value of a first-order polynomial function $f(x) = m\ x + b$ fitted to the current–voltage relationship near RMP. The τ_{memb} was determined by fitting a mono-exponential decay function to a voltage response elicited by injecting a negative current step (1 s, −30 pA). The membrane capacitance (C_m) was calculated as the ratio of τ_{memb} to R_N, as previously reported [22].

Determination of macroscopic currents

Whole-cell voltage-clamp configuration was performed to evoke total membrane currents by the injection of depolarizing pulses (−90 to +60 mV, 10-mV steps, 500 ms) from a holding potential of −70 mV. The P/4 protocol was employed to subtract leak currents online, and the recording quality was monitored online by incorporating the following criteria: holding currents < 50 pA, stable RMP, and access resistance (< 15 MW, < 20% drift). To generate I-V plots, the current amplitude was measured either at the maximum peak amplitude or as the average over a 100-msec interval at the steady-state current.

Statistical analysis

No statistical method was used to determine the sample size. The statistical analysis was performed with GraphPad Prism 8. The graphs represent the mean ± the standard error of the mean (SEM). The data normality was previously determined with a Kolmogorov-Smirnov test. Most of the data did not meet the normality criteria; and non-parametric tests were applied: Mann-Whitney U for comparing two experimental groups and Kruskal-Wallis for comparing more than two groups. A one-way analysis of variance (ANOVA) test was applied, followed by Tukey's post-hoc test in cases where normal distribution was observed. In cases where the comparison was between two groups, the Student's t-test was applied. In all cases, the accepted level of significance was set to $p < 0.05$ or a higher statistical significance.

Results

Progenitor markers and $GABA_B$ receptor subunits are co-expressed in neural progenitor cells of the subventricular zone

Neurospheres derived from neural precursor cells of the subventricular zone (NPC SVZ) were obtained from CD1 mice on postnatal day eight and cultured in a DMEM/F12 medium supplemented with B27(1%), EGF (20 nM), and FGF (20 nM). The expression of progenitor and proliferation markers was then determined. Fig 1A and 1B show secondary neurospheres expressing the progenitor marker nestin and the proliferation marker Ki-67, thus confirming the progenitor origin of the cultured cells. Next, we analyzed if secondary neurospheres expressed the G-protein coupled receptor for gamma-aminobutyric acid receptor B ($GABA_BR$). $GABA_BR$ is a metabotropic receptor assembled from two subunits: $GABA_{B1}$ and $GABA_{B2}$. Therefore, immunocytochemistry assays were individually performed against each receptor's subunit. Fig 1C and 1D show the immunoreactivity of $GABA_{B1}$ and $GABA_{B2}$, respectively. The $GABA_B$ subunits' presence indicates that secondary neurospheres derived from NPC SVZ expressed the metabotropic $GABA_B$ receptors in addition to the ionotropic $GABA_A$ receptors [23].

Activation of $GABA_AR$ with taurine induces neuronal differentiation and neurite outgrowth in NPC SVZ

We previously reported that disaggregated NPC SVZ incubated with taurine (14 days/10 mM) undergoes increased expression of neuronal markers accompanied by the development of passive and active electrophysiological properties [15]. The first observation was further investigated in the present study. The upper panels in Fig 2A show representative bright-field (10x) microphotographs of disaggregated NPC SVZ cultures in the control condition and incubated with taurine; the lower panels show immunofluorescence against doublecortin (DCX). Compared to the control condition, the taurine-treated cells exhibited an increased number of DCX+ cells (Mann Whitney test, U = 4; $p = 0.0019$, $n = 8$ for each experimental condition, Fig 2B) and increased development of somatic prolongations or neurites (Mann Whitney test, U = 426; $p < 0.001$; Fig 2C).

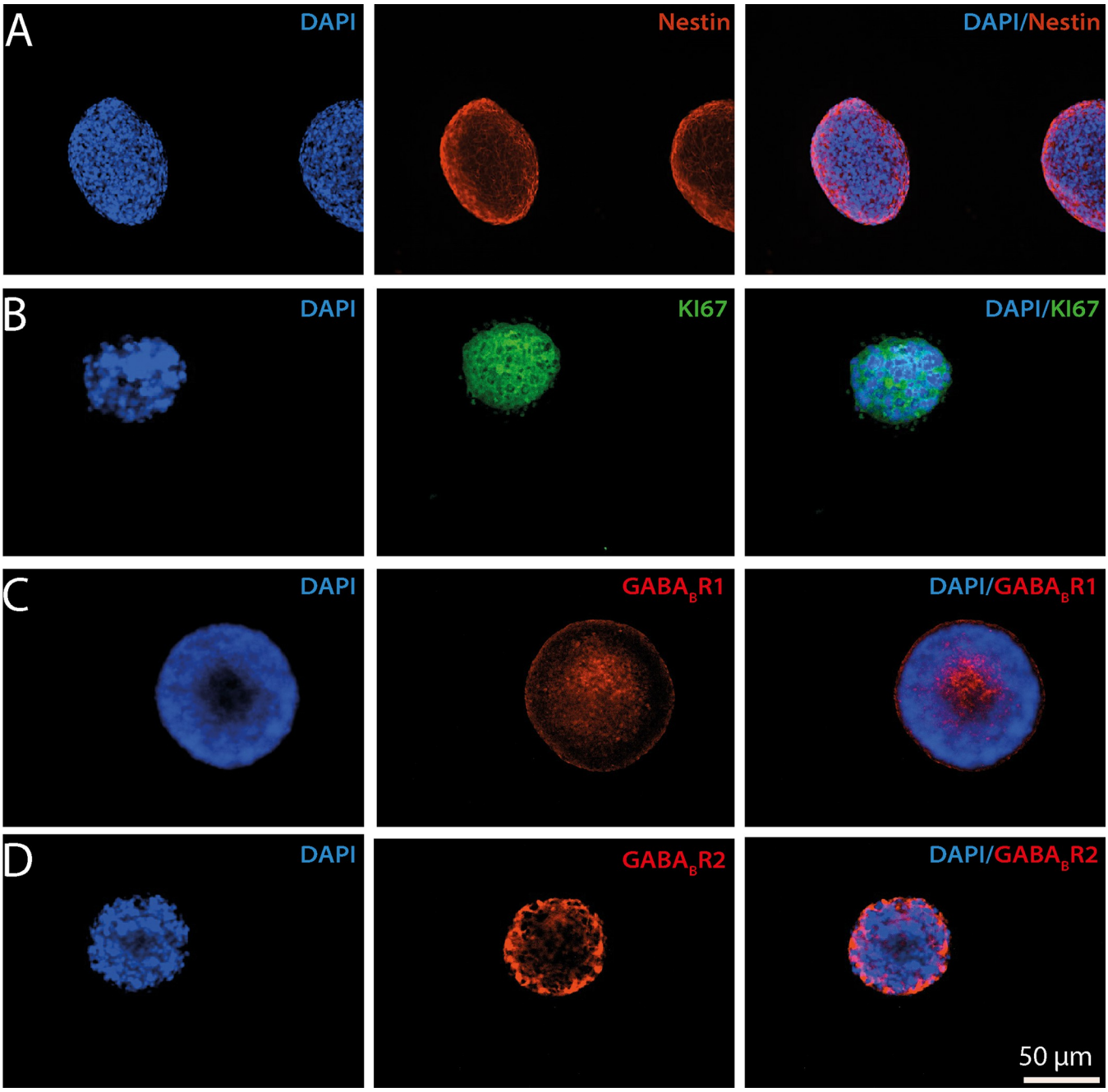

Fig 1. Expression of neural precursor cell markers and $GABA_B$ receptor subunits in secondary neurospheres derived from the subventricular zone. Microphotographs showing the immunoreactivity to precursor cell markers and $GABA_B$ subunits of cultured neurospheres. The secondary neurospheres exhibited a mean ratio of 70 ± 5 um. The nuclei of the proliferative cells within the neurosphere were labeled with DAPI staining. Immunoreactivity signals were detected for **A)** nestin (red) and **B)** KI67 (green), indicating the presence of neural progenitor cells and active proliferation, respectively. Likewise, the neurospheres exhibited immunoreactivity to the $GABA_B$ receptor subunits, **C)** $GABA_B$R1 (red), and **D)** $GABA_B$R2 (red). All the microphotographs were taken with a 20x magnification lens. The scale bar applies for all the panels.

https://doi.org/10.1371/journal.pone.0305853.g001

Next, a Sholl-like morphometric analysis was used to determine the pattern of neurite branching of the disaggregated cells treated with taurine. Digital reconstructions were performed from the bright-field microphotographs, and the resulting images were processed to trace neuronal arborizations. Fig 2F shows representative digital reconstructions of NPC SVZ

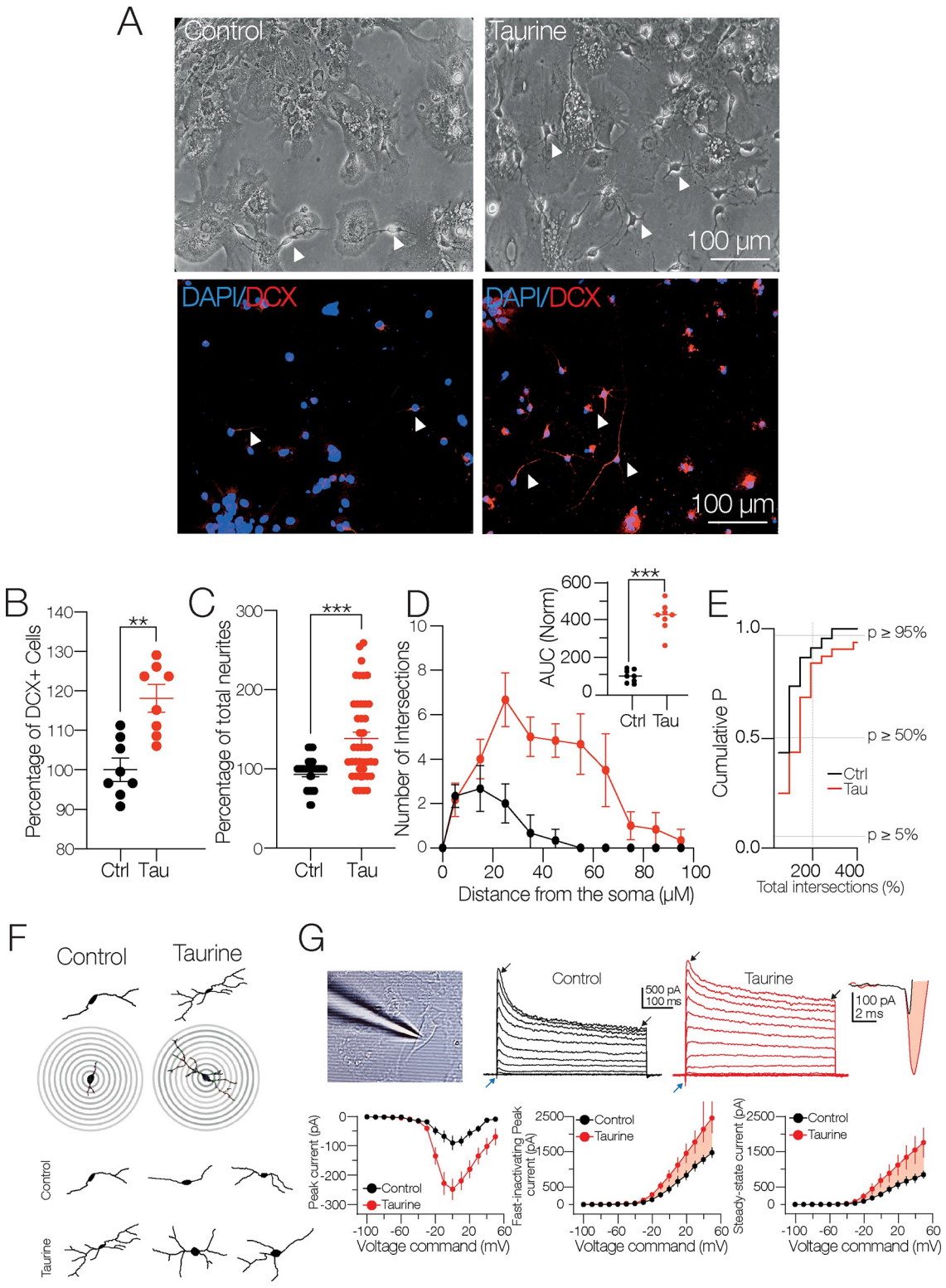

Fig 2. The interaction of the $GABA_A$ receptor and taurine promotes neurite outgrowth of NPC SVZ. A) Representative bright-field and immunofluorescence assays microphotographs against DCX for immature neurons in the control condition or in taurine (10 mM). The nuclei were stained with DAPI (blue) and DCX (red). Arrowheads indicate cells with neuronal-type morphology used for the analyses included in this study. **B)** Scatter plot showing the percentage of DCX+ cells in the control and in taurine (n = 8 cell cultures for each experimental condition). **C)** Scatter plot with the total number of neurites in the control condition (n = 36) and in

taurine (n = 40) DCX+ cells). **D)** Sholl-like analysis contrasting the number of neurite intersections in the control condition and the taurine-treated cells. Upper inset: area under the curve (AUC) chart showing the total area obtained from the Sholl-like analysis performed in the control and taurine-treated cells (n = 8 DCX+ cells). **E)** Cumulative probability chart summarizing the number of neurite intersections in the control cells versus the taurine-treated cells. The right shift of the taurine-treated cells mirrors the increased number of neurite intersections (n = 8 for each experimental condition). **F)** Upper panels: representative digital reconstructions and concentric rings (distance between rings = 10 μM) used for the Sholl-like morphometric analysis. Bottom panel: examples of the increased number of primary, secondary, and tertiary neurites of the taurine-treated cells. **G)** Left panel: a patch-clamp pipette attached to an NPC SVZ incubated with taurine. Notice the cell body and the neurite outgrowths. Middle panel: representative current traces obtained in a control and a taurine-treated cell. The blue arrowheads indicate the inward current, the black arrowheads indicate the fast-inactivating and the persistent, steady-state outward current. Right panel: magnification of the inward currents, black trace control, red trace, inward current of a taurine-treated cell. Bottom left panel: plot of the voltage dependence and maximal amplitude of the inward current. Middle panel: plot showing the maximal peak amplitude of the fast-inactivating outward current. Right panel: plot depicting the amplitude of the non-inactivating steady-state outward current. $^{**}p < 0.01$; $^{***}p < 0.001$ or higher statistical significance. Error bars indicate SEM.

https://doi.org/10.1371/journal.pone.0305853.g002

obtained in both experimental conditions and the overlapping concentric circles (distance = 10 μM) from which the values of the Sholl-like plot were obtained. The taurine-treated cells exhibited an increased number of neurite intersections compared to the control cells (Fig 2D and 2F). The increased number of intersections is summarized in the inset graph in Fig 2D, showing the area under the curve (AUC) obtained from the Sholl analysis (AUC in taurine-treated cells = 310.4 ± 39.4% compared with control AUC; t-test: $t_{(10)} = 7.875$; *** $p < 0.001$, n = 6 for each experimental condition). The cumulative probability chart in Fig 2E shows the distribution of the total number of intersections in the control cells and cells treated with taurine.

Morphologically, the control cells displayed bipolar-oriented somata with one or two primary neurites; by contrast, the taurine-treated cells exhibited a multipolar morphology with extensive neuritic arborizations and complex branching. Likewise, the number of neurites and intersections was significantly higher in the proximity of the somata of the taurine-treated cells (see representative examples in Fig 2F).

Next, we examined the functional expression of macroscopic currents expressed by the NPC SVZ using the whole-cell patch-clamp technique. Under the voltage-clamp mode, we applied a protocol (see methods for details) that sequentially elicited an inward current followed by an outward current. Taurine incubation dramatically increased the inward current compared to the control cells (inward current in the control condition = −76.2 ± 24 pA; in the taurine-treated cells = −248.1 ± 36.3 pA; t-test: $t_{(10)} = 3.63$; $p = 0.004$; n = 12 for each experimental condition; Fig 2G; blue arrowheads and far-right traces). On the other hand, the outward current exhibited two kinetic components: a fast-inactivating current peak followed by a steady, non-inactivating current that resembles the neuronal I_A and the I_D potassium currents [22, 24]. Interestingly, the taurine-treated cells exhibited an increased amplitude of the fast-inactivating outward current (fast-inactivating current in the control condition (n = 4) = 1,474.3 ± 150 pA; in the taurine-treated cells (n = 6) = 2,621.4 ± 42 pA; t-test: $t_{(8)} = 2.56$; $p = 0.03$; Fig 2G; black arrowheads in the middle panel current traces) and the steady, non-inactivating current (steady-state outward current in the control condition (n = 4) = 847 ± 111 pA; in the taurine-treated cells (n = 6) = 1,957.5 ± 421 pA; t-test: $t_{(8)} = 2.56$; $p = 0.03$; Fig 2G; black arrowheads in the middle panel current traces). Interestingly, the somatic input resistance (R_N) for the taurine-treated cells dropped ≈43% compared to the control cells (R_N in the control condition = 452.3 ± 55.49 MΩ; in the taurine-treated cells = 196.2 ± 17 MΩ; t-test; $t_{(10)} = 4.25$; $p < 0.001$; n = 12 for each experimental condition). Lastly, the relationship membrane time-constant / somatic input resistance ratio (τ_{memb}/R_N) yielded a membrane capacitance (C_m) of 47.39 ± 9.22 pF for the control and 41.47 ± 14.56 pF (*ns*) for the taurine-treated cells; t-test: $t_{(10)} = 1.02$; ns; n = 12 for each experimental condition; suggesting that the observed increase in the current amplitude was unrelated to changes in the somatic area.

Next, we corroborated that the pharmacological blockade of $GABA_AR$ decreases the neuronal differentiation process mediated by taurine [15]. Fig 3A shows bright-field microphotographs and the respective immunofluorescence assay against DCX performed in the control, the taurine-, and the taurine + picrotoxin (PTX, 100 μM)–treated cells. Fig 3B shows the decreased number of DCX+ cells in the presence of PTX (DCX+ cells in the presence of taurine = 117.9 ± 3.93%; one-way ANOVA; Tukey's test; $p < 0.01$; in the presence of taurine + PTX = 73.49 ± 3.93%; one-way ANOVA; Tukey's test; $p < 0.001$; $F_{(2, 21)} = 42.05$; $n = 8$ for each experimental condition). Consistent with this finding, Fig 3C shows a reduced number of neurites in the taurine + PTX condition (total number of neurites in the taurine-treated cells compared to the control cells ($n = 43$) = 138.3 ± 8.1%; one-way ANOVA; Tukey's test; $p < 0.001$; in taurine + PTX ($n = 23$) vs. the taurine-treated cells ($n = 43$) = 52.6 ± 7.6%; one-way ANOVA; Tukey's test; $p < 0.001$; $F_{(2, 106)} = 38.00$). Likewise, the blockade of $GABA_AR$ with PTX substantially decreased the intersections computed in the Sholl-like analysis (Fig 3D and 3F). This finding is summarized in the inset AUC graph (AUC in the presence of taurine = 310.4 ± 39.42%; one-way ANOVA; Tukey's test; $p < 0.001$; AUC in the presence of taurine + PTX = 81.25 ± 33.74%; one-way ANOVA; Tukey's test; $p < 0.001$ $F_{(2, 15)} = 60.05$; $n = 6$ for each experimental condition. The cumulative probability chart in Fig 3E shows the distribution of the total number of intersections in the three experimental conditions. Representative examples of the decreased neurite branching in response to the blockade of $GABA_AR$ with PTX are shown in the digital reconstructions (Fig 3F). The whole-cell patch clamp recordings revealed a series of changes in the amplitude of the macroscopic currents when $GABA_AR$ was blocked. Incubation of taurine + PTX decreased the maximal amplitude of the inward current compared to the taurine-treated cells (inward current in the taurine-treated cells = −-248.09 ± 36.30 pA; in the taurine + PTX–treated cells = −32.42 ± 11.66 pA; t-test: $t_{(10)} = 5.65$; $p = 0.0002$; $n = 12$ for each experimental condition; Fig 3G; blue arrowheads and far-right traces). On the other hand, both the fast-inactivating and the steady-state outward currents exhibited a decreased amplitude in the presence of PTX (fast-inactivating current in the taurine-treated cells = 2,154.5 ± 422.03 pA; in the presence of taurine + PTX = 1,057.1 ± 129.8 pA; t-test: $t_{(10)} = 4.24$; $p = 0.001$; $n = 12$ for each experimental condition; steady-state outward current in the taurine-treated cells = 1,557.5 ± 421 pA; in the presence of taurine + PTX = 617.45 ± 106.6 pA; t-test: $t_{(10)} = 3.49$; $p = 0.005$; $n = 12$ for each experimental condition; Fig 3G; white arrowheads in the middle panel current traces). In the taurine + PTX–treated cells, the R_N did not exhibit a significant change compared to the control cells (R_N in the taurine-treated cells ($n = 6$) = 204.6 ± 18.2 MΩ; in taurine + PTX ($n = 5$) = 513.5 ± 114 MΩ; t-test: $t_{(9)} = 2.95$; $p = 0.01$). No changes were found in the C_m of the taurine + PTX–treated cells compared to the taurine-treated cells (C_m in the taurine-treated cells ($n = 6$) = 47.39 ± 9.22 pF; in taurine + PTX ($n = 5$) = 55.10 ± 18.13 pF; t-test: $t_{(9)} = 1.84$; ns). Collectively, these experiments indicate that activation of the $GABA_AR$ is necessary for the morphogenic process, neurite development, and functional expression of ion channels mediated by taurine.

Activation of $GABA_B$ receptors does not stimulate the differentiation process of NPC SVZ

Because secondary neurospheres express both subunits of the $GABA_BR$ (see Fig 1C and 1D), we next determined the role of the metabotropic $GABA_BR$ in the differentiation process of NPC SVZ. The cultures were exposed to the $GABA_BR$ agonist baclofen (100 μM) in the presence of taurine (10 mM/14 days), and the expression of DCX was evaluated. Fig 4A shows bright-field microphotographs and the respective immunofluorescence assays against DCX in the control, the taurine-, and the taurine + baclofen–treated cells. Activation of $GABA_BR$ with

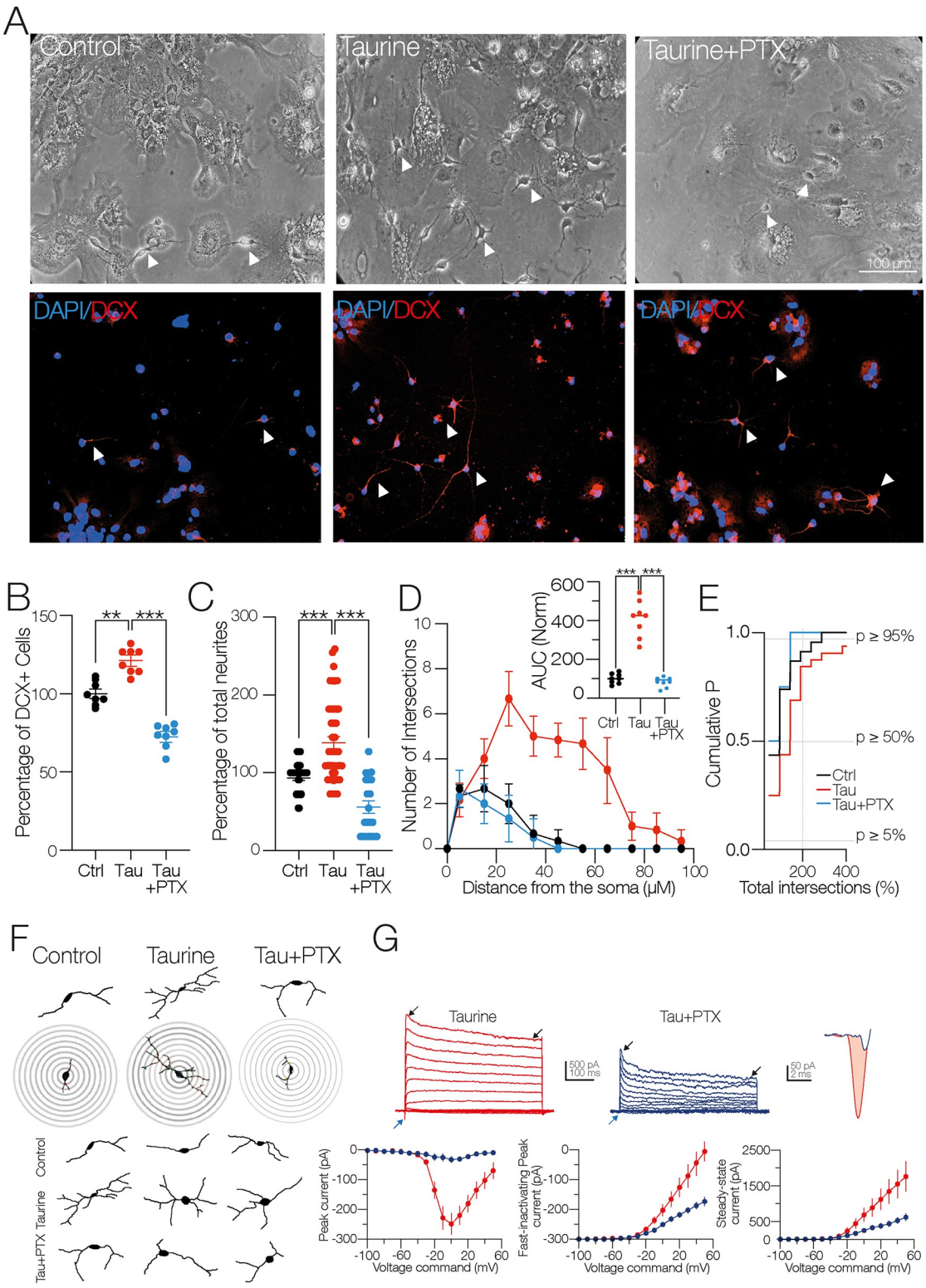

Fig 3. Pharmacological blockade of $GABA_A$ receptor inhibits neurite outgrowth of NPC SVZ. A) Bright-field and immunofluorescence assays. Nuclei were stained with DAPI (blue) and DCX (red). Arrowheads show cells with a neuronal-type morphology obtained in the indicated experimental conditions. **B)** Scatter plot summarizing the percentage of DCX+ cells in the control and in the presence of taurine and taurine + PTX (n = 8 cell cultures for each experimental condition). **C)** Scatter plot showing the total number of neurites in the indicated experimental conditions. PTX prevented the neurite outgrowth observed

stimulated with taurine (control $n = 34$ cells; taurine $n = 38$ cells; taurine + PTX $n = 27$ DCX+ cells). **D)** Sholl-like analysis with the number of neurite intersections in the indicated experimental conditions. Upper inset: AUC chart summarizing the findings of the Sholl-like analysis ($n = 8$ DCX+ cells). **E)** Cumulative probability chart. The left shift of the taurine + PTX–treated cells (blue line) mirrors the decreased number of neurite intersections when $GABA_A$ receptors were blocked (control $n = 34$ cells; taurine $n = 38$ cells; taurine + PTX $n = 27$ DCX+ cells). **F)** Representative digital reconstructions and concentric rings used for the Sholl-like analysis. Notice the decreased number of primary, secondary, and tertiary neurites of the taurine + PTX–treated cells (right panel). **G)** Upper panel: representative current traces obtained from cells treated with taurine or taurine + PTX. Blue arrowheads indicate the inward currents, black arrowheads the fast-inactivating and the persistent, steady-state outward current. Upper right panel: magnification of the inward current from a taurine-treated cell (red trace) and a taurine + PTX–treated cell (blue trace). Bottom left panel: voltage dependence and maximal amplitude of the inward current. Middle panel: the maximal amplitude of the fast-inactivating outward current. Right panel: the steady-state amplitude of the non-inactivating outward current. ns = non-significant statistical difference; $^{**}p < 0.01$; $^{***}p < 0.001$ or higher statistical significance. Error bars indicate SEM.

https://doi.org/10.1371/journal.pone.0305853.g003

baclofen + taurine did not modify the number of DCX+ cells compared to the taurine-treated cells (number of DCX+ cells in the presence of taurine compared to the control cells = 117.9 ± 4.38%; one-way ANOVA; Tukey's test; $p < 0.01$; in the presence of taurine + baclofen compared with the taurine-treated cells = 106.3 ± 4.38%; ns; $F_{(2, 20)} = 8.33$; $n = 8$ for each experimental condition; Fig 4B). Moreover, the activation of $GABA_BR$ with baclofen decreased the number of neurites (total number of neurites in taurine compared to the control cells ($n = 43$) = 138.3 ± 8.1%; one-way ANOVA; Tukey's test; ns; in taurine + baclofen ($n = 20$) compared with the taurine-treated cells ($n = 43$) = 83.1 ± 7.7%; one-way ANOVA; Tukey's test; $p < 0.001$; $F_{(2, 118)} = 20.38$; Fig 4C). Likewise, the neurite intersections were also decreased in the taurine + baclofen condition, as shown in Fig 4D and the inset and the concentric circles of the Sholl-like plot analysis in Fig 4F (AUC in the presence of taurine compared to the control cells = 310.1 ± 40%; one-way ANOVA; Tukey's test; $p < 0.001$; AUC in the presence of taurine + baclofen compared with the taurine-treated cells = 189.6 ± 37.5%; one-way ANOVA; Tukey's test; $p < 0.001$).

The cumulative probability chart in Fig 4E shows the distribution of the total number of intersections in the three experimental conditions. Morphologically, the cells treated with taurine + baclofen exhibited similar characteristics to the control cells, including short and few neurite outgrowths (Fig 4F). The lack of action of the $GABA_BR$ stimulation was mirrored in the amplitude of the inward current (inward current in the taurine-treated cells ($n = 6$) = −-248.09 ± 36.30 pA; in the taurine + baclofen–treated cells ($n = 3$) = −64.99 ± 41.94 pA; t-test: $t_{(7)} = 3.24$; $p = 0.001$; Fig 4G; blue arrowheads and far-right traces) and outward current's components (fast-inactivating current in the taurine-treated cells ($n = 6$) = 2,154.5 ± 422 pA; in the presence of taurine + baclofen ($n = 3$) = 1,070 ± 450 pA; t-test: $t_{(7)} = 2.13$; $p = 0.06$; (*ns*); steady-state outward current in the taurine-treated cells ($n = 6$) = 1,557.5 ± 421 pA; in the presence of taurine + baclofen ($n = 3$) = 550 ± 207 pA; t-test: $t_{(7)} = 2.07$; $p = 0.08$; *ns*; Fig 4G); white arrowheads in the middle panel current traces). In the presence of tau + baclofen, the R_N showed a significant change compared to the taurine-treated cells (R_N in the taurine-treated cells ($n = 6$) = 190.8 ± 19.7 MΩ; in the taurine + baclofen–treated cells ($n = 3$) = 463.3 ± 66 MW; t-test: $t_{(7)} = 5.49$; $p = 0.001$).

No changes were found in the C_m of the taurine + baclofen–treated cells compared to taurine-treated cells (C_m in the taurine-treated cells ($n = 6$) = 48.1 ± 9.22 pF; in taurine + baclofen ($n = 3$) = 43.84 ± 11.42 pF; t-test: $t_{(7)} = 1.55$; ns). Collectively, these results demonstrate that baclofen-induced $GABA_BR$ activation does not contribute to the neuronal differentiation process of the NPC SVZ or to the balanced expression of macroscopic currents; on the contrary, $GABA_BR$ activation appears to interfere with neurite outgrowth and the functional expression of ion channels.

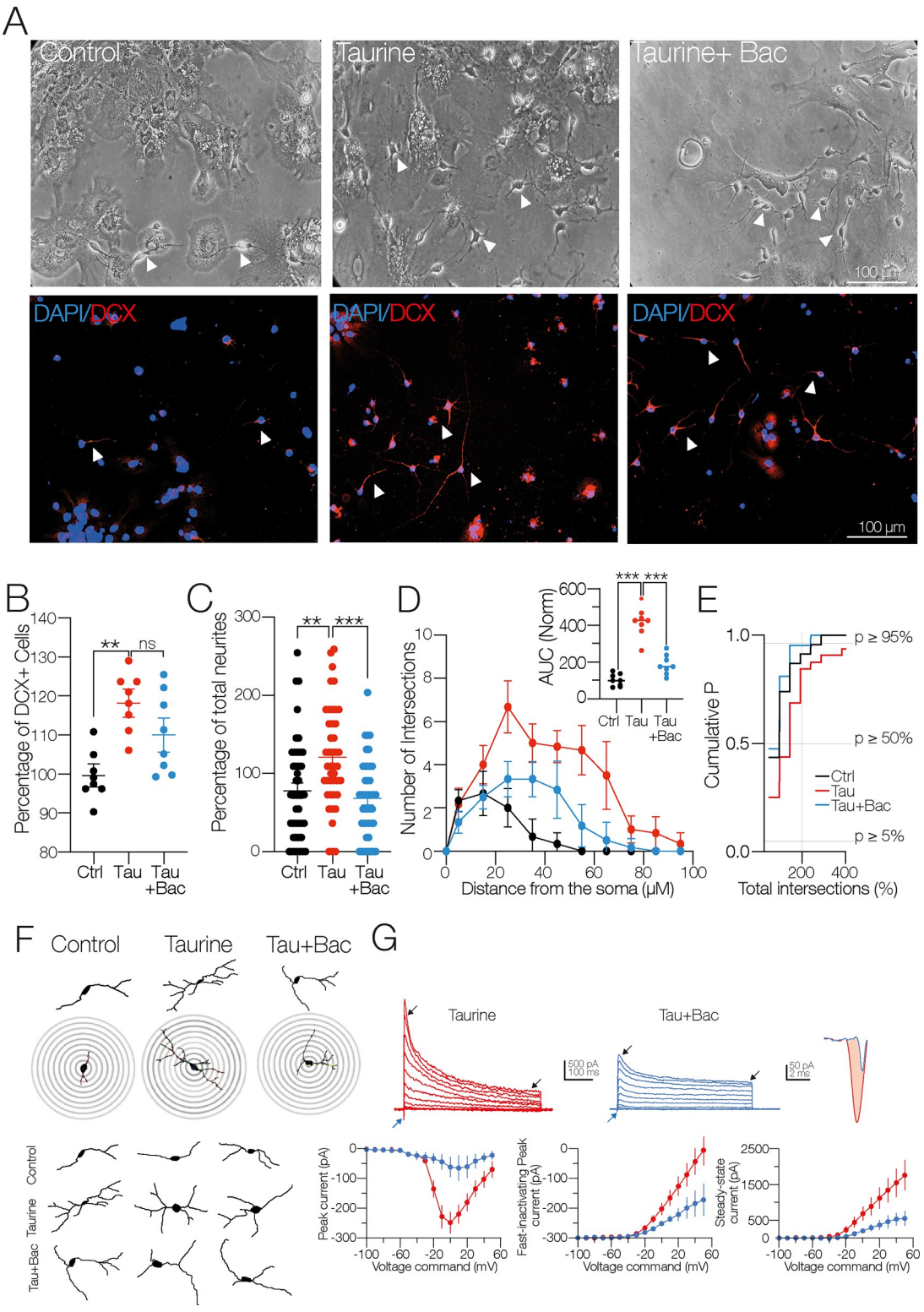

Fig 4. Activation of the $GABA_B$ receptor with baclofen does not stimulate the differentiation process of NPC SVZ. A) Bright-field and immunofluorescence assays microphotographs for DCX in the control cells, taurine (10mM), and taurine + baclofen (100 μM)–treated cells. Nuclei were stained with DAPI (blue) and DCX (red). Arrowheads show cells with a neuronal-type morphology obtained in the indicated conditions. **B)** Scatter plot showing the percentage of DCX+ cells in the indicated experimental conditions. Stimulation with baclofen did not alter the number of DCX+ cells (n = 8 cell cultures for each

experimental condition). **C)** Comparison of the total number of neurites in the indicated experimental conditions. The combination of taurine + baclofen did not stimulate neurite outgrowths compared to the taurine-treated cells (control $n = 33$ cells; taurine $n = 43$ cells; taurine + baclofen $n = 37$ DCX+ cells). **D)** Sholl-like analysis obtained from the indicated experimental conditions. Upper inset: AUC chart summarizing the findings of the Sholl-like analysis ($n = 8$ DCX+ cells). **E)** Cumulative probability chart of the number of neurite intersections in the three experimental conditions (control $n = 33$ cells; taurine $n = 43$ cells; taurine + baclofen $n = 37$ DCX+ cells). **F)** Digital reconstructions and concentric rings used for morphometric analyses. Notice the subtle changes in the number of primary, secondary, and tertiary neurites of the taurine + baclofen–treated cells (right panel). **G)** Upper panel: representative current traces obtained from cells treated with taurine or taurine + baclofen. Blue arrowheads indicate the inward currents, black arrowheads the fast-inactivating and the persistent, steady-state outward current. Upper right panel: magnification of the inward current from a taurine-treated cell (red trace) and taurine + baclofen–treated cell (blue trace). Bottom left panel: voltage dependence and maximal amplitude of the inward current. Middle panel: the maximal amplitude of the fast-inactivating outward current. Right panel: the steady-state amplitude of the non-inactivating outward current. ns = non-statistical significance; $^{**}p < 0.01$; $^{***}p < 0.001$ or higher statistical significance. Error bars indicate SEM.

https://doi.org/10.1371/journal.pone.0305853.g004

Blockade of the $GABA_B$ receptors favors the neuronal differentiation process, complexity, and the number of neurites of NPC SVZ

Next, we explored the effects of the blockade of $GABA_BR$ in the differentiation process. NPC SVZ were exposed to the selective $GABA_BR$ antagonist CGP 55845 (5 μM) in the presence of taurine (10 mM/14 days), and the expression of DCX was evaluated. Bright-field microphotographs and immunofluorescence assays against DCX performed in the control, taurine-, and taurine + CGP 55845–treated cells are shown in Fig 5A. Strikingly, the blockade of $GABA_BR$ with CGP 55845 increased the number of DCX+ cells by a similar amount as the observed with taurine (DCX+ cells in the presence of taurine compared to the control cells = 117.9 ± 3.60%; one-way ANOVA; Tukey's test; p 0.0002; in the presence of CGP 55845 + taurine compared to the taurine-treated cells = 117.2 ± 3.60%; one-way ANOVA; Tukey's test; $p = 0.9775$; $F_{(2, 21)} = 15.37$; $n = 8$ for each experimental condition; Fig 5B). Likewise, these cells exhibited a higher number of neurites (total number of neurites in the presence of taurine compared to the control cells ($n = 43$) = 138.3 ± 8%; one-way ANOVA; Tukey's test; $p < 0.001$; in the presence of taurine + CGP 55845 ($n = 30$) compared to the taurine-treated cells ($n = 43$) = 127.2 ± 8.6; one-way ANOVA; Tukey's test; p 0.033; ns; $F_{(2, 13)} = 13.07$; Fig 5C). Additionally, the blockade of $GABA_BR$ increased the number of neurite intersections (Fig 5D and the concentric circles of the Sholl-like plot in Fig 5F). The increased intersection number in response to CGP 55845 + taurine is summarized in the inset graph (AUC in the presence of taurine compared to the control cells = 310.4 ± 40%; one-way ANOVA; Tukey's test; $p < 0.001$; AUC in the presence of taurine + CGP 55845 compared to the taurine-treated cells = 516.7 ± 45.55%; one-way ANOVA; Tukey's test; $p < 0.001$; $F_{(2, 15)} = 65.19$; $n = 6$ for each experimental condition). The cumulative probability chart in Fig 5E shows the distribution of the total number of intersections in the control, in cells treated with taurine, and in cells treated with taurine + CGP 55845. Morphologically, the neurites of the CGP 55845–treated cells exhibited a robust neuronal-like morphology, with complex neurite outgrowth and a more intricate branching pattern than those observed in the taurine-treated group. Interestingly, the amplitude of the inward currents did not increase in the presence of CGP 55845 (inward current in the taurine-treated cells ($n = 6$) = −248.09 ± 36.30 pA; in the taurine + CGP 55845–treated cells ($n = 3$) = −29.78 ± 2.84 pA; t-test: $t_{(7)} = 4.11$; $p = 0.004$;Fig 5G; blue arrowheads and far-right traces). On the other hand, the amplitude of the fast-inactivating, and the persistent current decreased in the presence of CGP 55845 (fast-inactivating current in the taurine-treated cells ($n = 6$) = 2,050.4 ± 142 pA; in the presence of taurine + CGP 55845 ($n = 3$) = 978.41 ± 181 pA; t-test: $t_{(7)} = 4.24$; $p = 0.01$; steady-state outward current in the taurine-treated cells ($n = 6$) = 1,559 ± 421 pA; in the presence of taurine + CGP 55845 ($n = 3$) = 1,219.26 ± 171 pA; t-test: $t_{(7)} = 1.31$; $p = 0.23$; Fig 4G). Regarding the R_N, the tau + CGP 55845

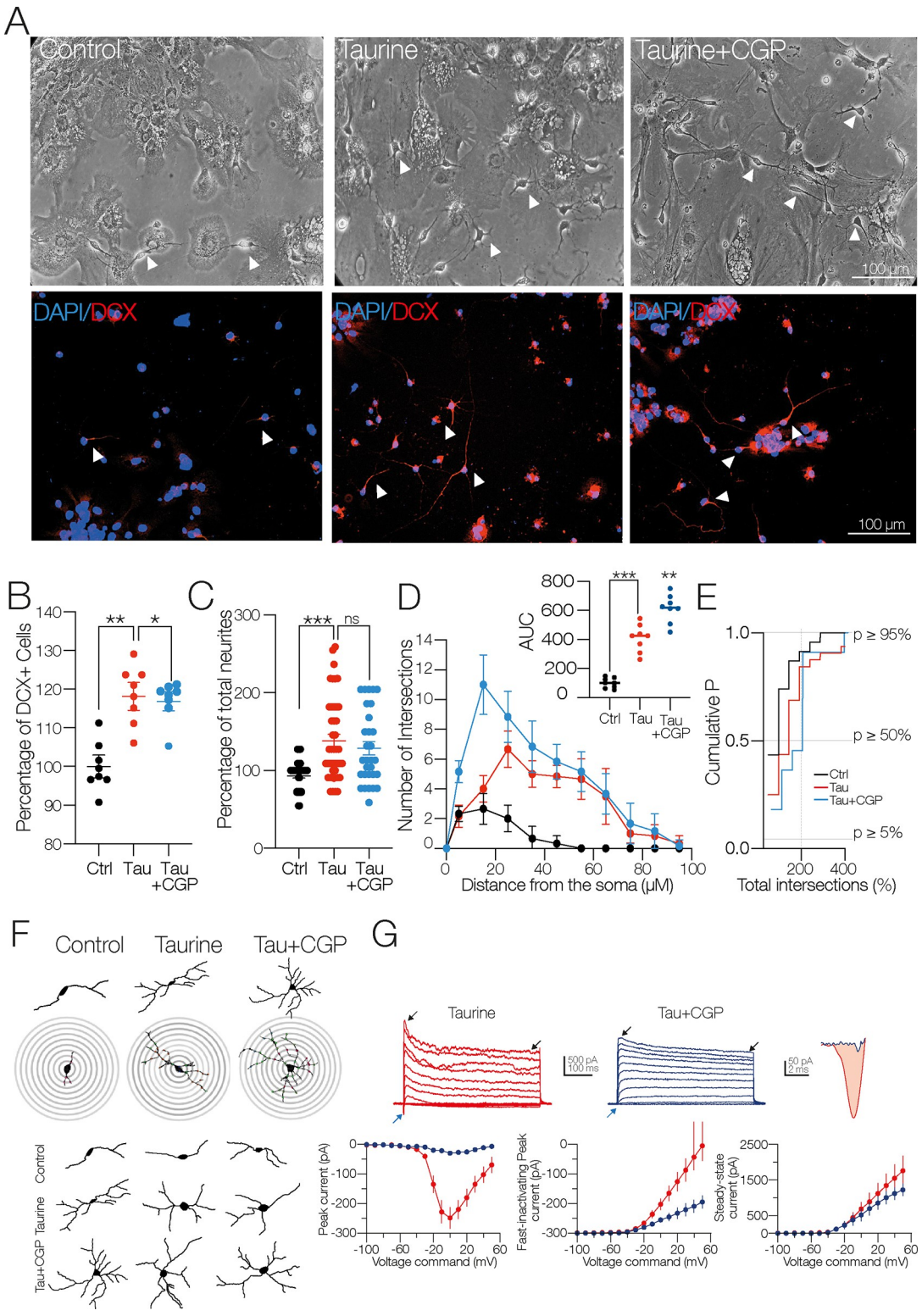

Fig 5. The blockade of $GABA_B$ receptors with CGP 55845 favors the differentiation process and neurite outgrowth of NPC SVZ. A) Bright-field and immunofluorescence assays microphotographs for DCX in the control condition, taurine, and taurine + CGP 55845 (5 μM). Arrowheads indicate cells with a neuronal-type morphology. **B)** Scatter plot summarizing the percentage of DCX+ cells in the indicated experimental conditions (n = 8 cell cultures for each experimental condition). **C)** Scatter plot summarizing the percentage of total neurites. Taurine + CGP 55845 increased the total number of neurites (control n = 38 cells;

taurine $n = 47$ cells; taurine + CGP 55845 $n = 43$ DCX+ cells). **D)** Sholl-like plot contrasting the number of intersections in the indicated experimental conditions. Upper inset: AUC chart ($n = 8$ cells for each experimental condition). **E)** Cumulative probability chart summarizing the number of neurite intersections. The right shift of the taurine + CGP 55845–treated cells mirrors the increased number of neurite intersections ($n = 6$ DCX+ cells). **F)** Representative digital reconstructions and concentric rings. Notice the increased number of primary, secondary, and tertiary neurites of the taurine + CGP 55845–treated cells. **G)** Upper panel: representative current traces obtained from NPC SVZ treated with taurine or taurine + CGP 55845. Blue arrowheads indicate the inward currents, black arrowheads the fast-inactivating and the persistent, steady-state outward current. Upper right panel: magnification of the inward current from a taurine-treated cell (red trace) and a taurine + CGP 55845–treated cell (blue trace). Bottom left panel: voltage dependence and maximal amplitude of the inward current. Middle panel: the maximal amplitude of the fast-inactivating outward current. Right panel: the steady-state amplitude of the non-inactivating outward current. ns = non-statistical significance; $^{*}p < 0.05$; $^{**}p < 0.01$; $^{***}p < 0.001$ or higher statistical significance. Error bars indicate SEM.

https://doi.org/10.1371/journal.pone.0305853.g005

treatment caused a slight drop (≈19%) compared to the control cells (R_N in the taurine condition ($n = 6$) = 465 ± 55 ΩOhm; in the taurine + CGP 55845–treated cells ($n = 4$) = 379.5 ± 52 ΩOhm; t-test: $t_{(8)} = 3.14$; $p = 0.01$). No changes were found in the Cm of the cells treated with CGP 55845 (C_m in the taurine-treated cells ($n = 6$) = 47.39 ± 9.22 pF; in taurine + CGP 55845 ($n = 4$) = 53.48 ± 12.1 pF; t-test: $t_{(8)} = 1.94$; ns). These findings demonstrate that the blockade of the metabotropic $GABA_BR$ enhances the morphogenic process of NPC SVZ with limited effects on the functional expression of macroscopic currents. The latter finding requires additional investigation.

A rise in intracellular calcium is necessary for the neuronal differentiation process mediated by taurine

Because taurine is a well-known modulator of intracellular Ca^{2+} homeostasis (Wu and Prentice, 2010) we explored if calcium mobilization is involved in the morphogenic process of NPC SVZ mediated by taurine. To test this hypothesis, the cultures were preincubated with taurine + BAPTA-AM. As expected, the intracellular Ca^{2+} chelation with BAPTA-AM significantly reduced the number of neurites mediated by taurine (total number of neurites in the presence of taurine ($n = 41$) for each experimental condition compared to the control cells ($n = 40$) for each experimental condition = 138.3 ± 7.5%; $p < 0.001$; in the presence of taurine + BAPTA-AM ($n = 23$) for each experimental condition compared to the taurine-treated cells = 35.16 ± 7.6%. $p < 0.001$; one-way ANOVA., Tukey's test; $F_{(2, 101)} = 29.60$; Fig 6A). Likewise, BAPTA-AM decreased the total length of the neurites of the taurine-treated cells (total length of neurites in the presence of taurine ($n = 91$) = 27.4 ± 1.5 μm; $p < 0.001$; in the presence of taurine + BAPTA-AM ($n = 29$) = 11.5 ± 2 μm; $p < 0.001$. one-way ANOVA; Tukey's test; $F_{(2, 194)} = 20.07$; Fig 6B). The effects of BAPTA-AM on the neurite outgrowth are shown in the Sholl-like plots (Fig 6C) and summarized in the AUC graph (AUC in the presence of taurine compared to the control cells = 410.4 ± 32.44%; $p < 0.001$; in the presence of taurine + BAPTA-AM compared to taurine cells = 127.1 ± 32.44%; $F_{(2, 15)} = 56.17$; $n = 8$ for each experimental condition; Fig 6D).

We also performed an immunoreactivity assay against the microtubule-associated protein 2 (MAP2) in the cultures exposed to taurine + BAPTA-AM. Immunoreactivity to MAP2 is a strong indicator of stable neuronal morphology during neuronal maturation. In addition to affecting neurite outgrowth, we hypothesized that Ca^{2+} chelation with BAPTA would negatively affect neuronal maturation. As expected, BAPTA-AM decreased the MAP2 immunoreactivity (MAP2+ immunoreactivity in the presence of taurine compared to the control cells = 134.6 ± 13.3; $p = 0.0525$; ns; in the presence of taurine + BAPTA-AM = 69.90 ± 8.31%; $p < 0.001$; one-way ANOVA; Tukey's test; $F_{(2, 15)} = 23.53$; $n = 6$ for each experimental condition; Fig 6E). Collectively, these experiments demonstrate that the differentiation and maturation process of NPC SVZ mediated by taurine involves intracellular calcium mobilization.

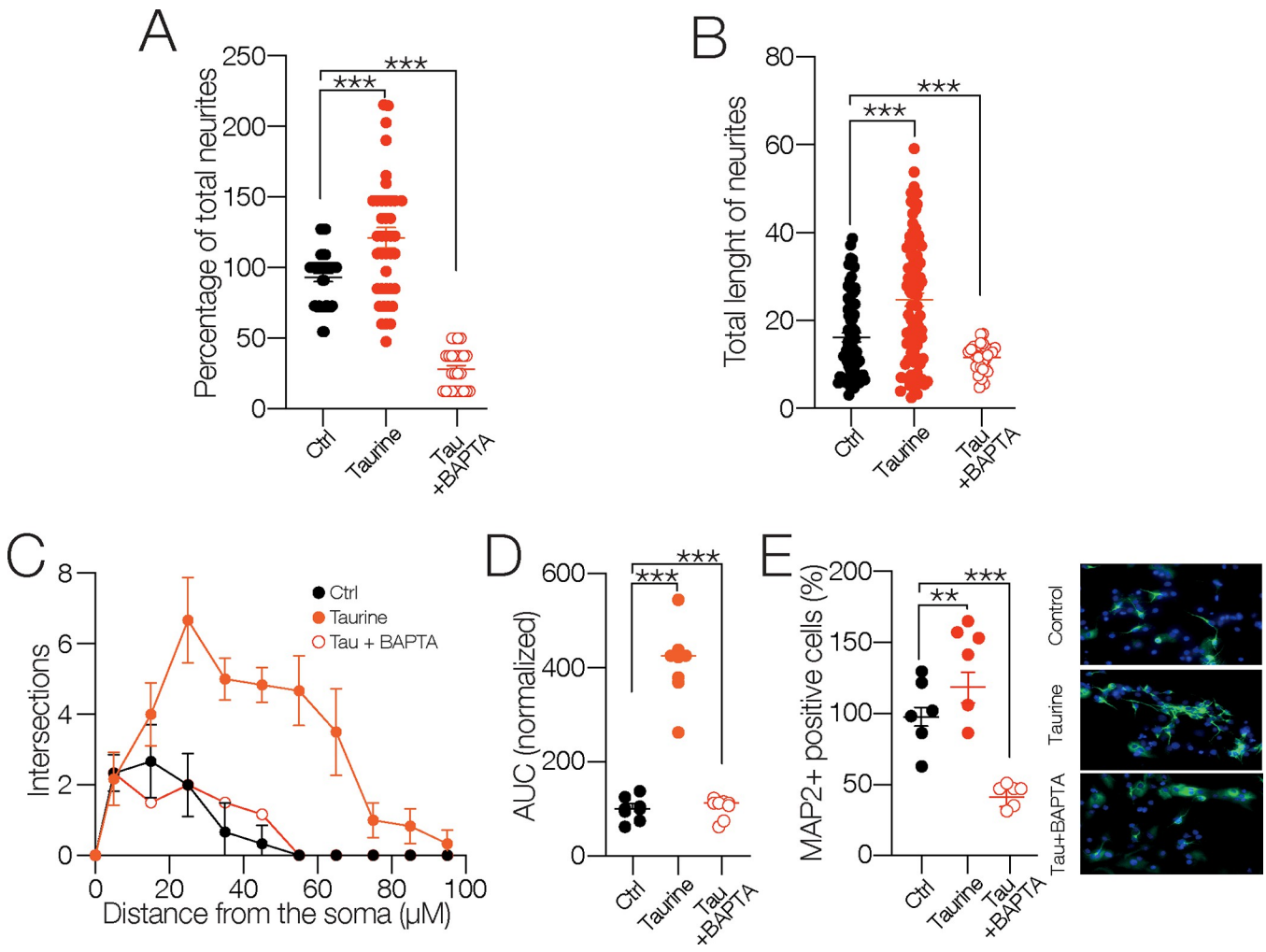

Fig 6. Taurine involves intracellular calcium mobilization for the differentiation process and neurite outgrowth of NPC SVZ. A) Scatter plot showing the number of neurites of NPC SVZ exposed to taurine or taurine + BAPTA-AM. Intracellular calcium chelation prevented neurite outgrowth. **B)** Scatter plot showing neurite length in the indicated experimental conditions. BAPTA incubation inhibited neurite outgrowth stimulated with taurine (control $n = 31$ cells; taurine $n = 36$ cells; taurine + BAPTA-AM $n = 12$ MAP2+ cells). **C)** Sholl-like plot contrasting the number of intersections in the indicated experimental conditions. **D)** AUC chart summarizing the findings of the Sholl-like analysis ($n = 6$ MAP2+ cells). **E)** Immunofluorescence assay microphotographs against MAP2 in taurine- and taurine + BAPTA–treated cells. BAPTA treatment reduced immunoreactivity to MAP2 ($n = 6$ cells for each experimental condition). ns = non-statistical significance; $^{**}p < 0.01$; $^{***}p < 0.001$ or higher statistical significance. Error bars indicate SEM.

https://doi.org/10.1371/journal.pone.0305853.g006

To culminate this study, we investigated the role of Ca^{2+}-dependent signaling cascades. The cultures were preincubated with taurine combined with the calcium–calmodulin (CaM)–dependent protein kinase II (CaMKII) inhibitor KN93, the extracellular-signal-regulated kinase (ERK1/2) inhibitor FR1805, and the Src-family protein-tyrosine kinase inhibitor Srcl. The blockade of CaMKII, ERK1/2, and Srcl inhibited the formation of neurites stimulated with taurine (total number of neurites in the presence of taurine ($n = 41$) compared to the control cells ($n = 41$) = 98.43 ± 6.55 μm; $p = 0.911$; in the presence of taurine + KN93 ($n = 26$) = 27.80 ± 7.42%; $p < 0.001$; in the presence of taurine + FR1805 ($n = 21$) = 37.98 ± 7.94%; $p < 0.001$; in the presence of taurine + Srcl ($n = 19$) = 44.6 ± 8.21%; $p < 0.001$; one-way ANOVA; Tukey's test; $F_{(4, 142)} = 38.39$; Fig 7A) and inhibited the increase in their length (total length of neurites in the presence of taurine ($n = 77$) compared to the control cells ($n = 91$) = 24.7 ± 1.6 μm; $p < 0.001$; in the presence of taurine + KN93 ($n = 29$) = 98.43 ± 4 μm $p < 0.001$;

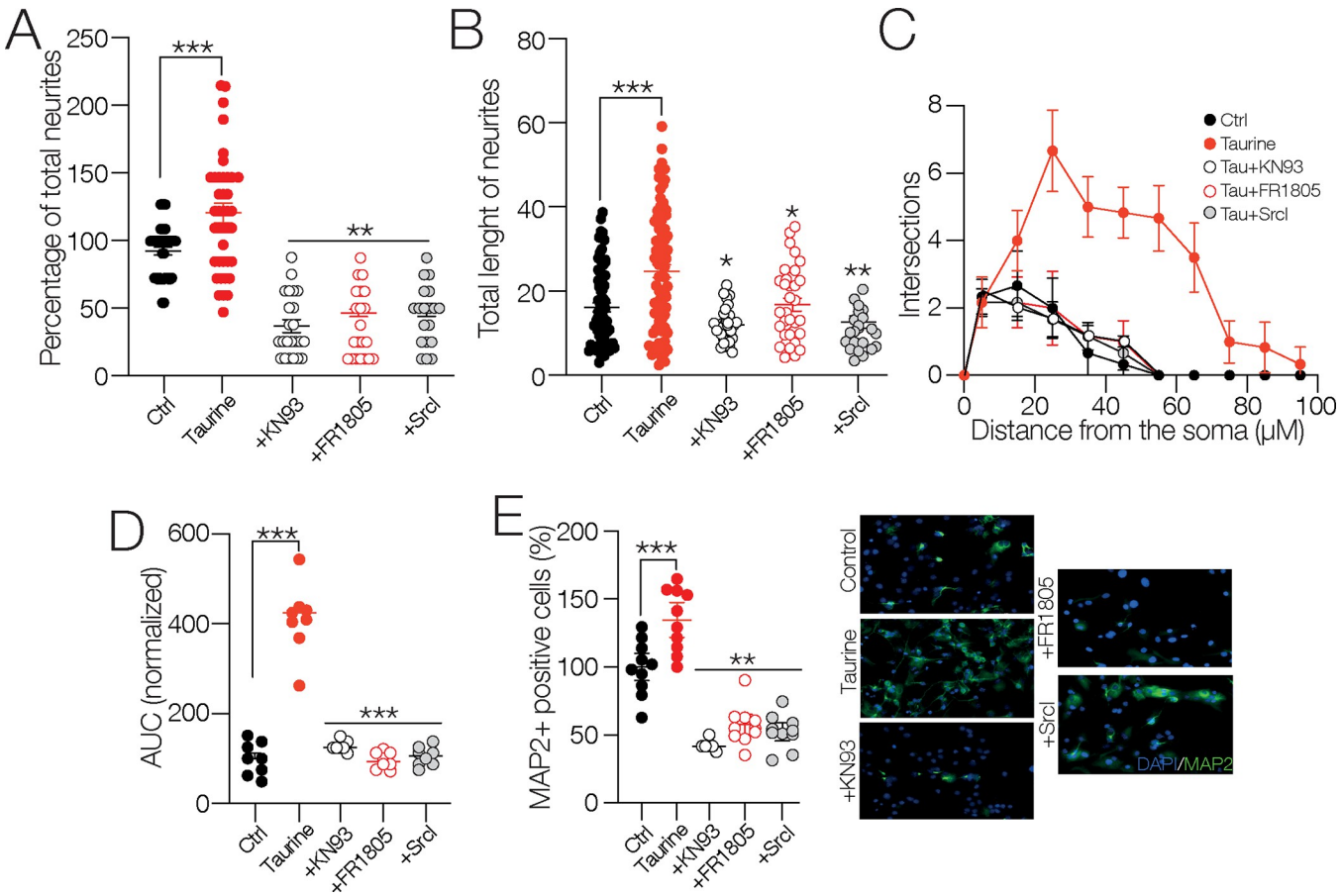

Fig 7. Involvement of signaling cascades in the differentiation process and neurite outgrowth of NPC SVZ mediated by taurine. A, B) Scatter plots showing the total number (A) and total length of neurites (B) of NPC SVZ treated with taurine or taurine + the CaMKII inhibitor KN93, taurine + the ERK1/2 kinase inhibitor FR1805, and taurine + the Src kinase inhibitor Srcl. The blockade of these signaling cascades prevented the neurite outgrowth promoted with taurine (control $n = 25$ cells; taurine $n = 42$ cells; taurine + KN93 $n = 15$ cells; taurine + FR1805 $n = 16$ cells; taurine + SrcI $n = 19$ MAP2+ cells). **C)** Sholl-like plot contrasting the number of neurite intersections in the control condition and the blockade of the indicated signaling cascades ($n = 6$ MAP2+ cells). **D)** AUC chart showing the total area obtained from the Sholl-like analysis performed in the control cells, in cells treated with taurine, and following the blockade of the indicated signaling cascades ($n = 6$ MAP2+ cells for each experimental condition). **E)** Immunofluorescence assay microphotographs against MAP2 in taurine and taurine + the signaling cascade blockers. The nuclei were stained with DAPI (blue). The blockade of CaMKII, ERK½, or Src kinase reduced the immunoreactivity to MAP2 ($n = 6$ cell cultures for each experimental condition). $^{**}p < 0.01$; $^{***}p < 0.001$ or higher statistical significance. Error bars indicate SEM.

https://doi.org/10.1371/journal.pone.0305853.g007

in the presence of taurine + FR1805 ($n = 33$) = 16.7 ± 2.2 μm; $p < 0.003$; in the presence of taurine + SrcI ($n = 26$) = 12.8 ± 2.5 μm; $p < 0.001$; one-way ANOVA; Tukey's test; $F_{(4, 248)} = 12.03$; Fig 7B). Likewise, the inhibition of the signaling cascades impacted the number of intersections plotted in the Sholl-like analysis (Fig 7C) and the resulting AUC (AUC in the presence of taurine compared to the control cells = 410.4 ± 24.6%; $p < 0.001$; in the presence of taurine + FR1805 = 95.9 ± 24.6%; $p < 0.001$; in the presence of taurine + SrcI = 106.3 ± 24.6%; $p < 0.001$; one-way ANOVA; Tukey's test; $n = 6$ for each experimental condition; $F_{(4, 25)} = 54.46$; Fig 7D). Consistent with these findings, the immunoreactivity of MAP2 kinase was dramatically decreased when these signaling cascades were blocked (MAP2+ cells in the presence of taurine compared to the control cells = 134.6 ± 13.3%; $p = 0.099$; ns; in the presence of taurine + KN93 = 61.6 ± 12%; $p < 0.001$; in the presence of taurine + FR1805 = 57.5 ± 13.3%; $p < 0.001$; in the presence of taurine + SrcI = 52.3 ± 13.3%; $p < 0.001$; one-way ANOVA; Tukey's test; $F_{(4, 25)} = 15.05$; $n = 6$ for each experimental condition; Fig 7E). Collectively, these

results demonstrate that CaMKII, ERK1/2, and the Src kinase play a crucial role in the taurine-mediated neuronal differentiation process. More specifically, inhibition of these signaling cascades negatively impacts the morphology and complexity of the differentiation process of the NPC SVZ.

Discussion

The results of this study are summarized as follows: We have provided evidence that taurine, by interacting with $GABA_A$- or $GABA_B$ receptors, controls the differentiation process, neurite formation, and functional expression of ionic currents of NPC SVZ. First, we demonstrated the presence of the $GABA_B$ receptor subunits, $GABA_BR1$ and $GABA_BR2$, in NPC SVZ derived from neurospheres immunopositive to nestin and Ki-67, which are progenitor and proliferation cell markers, respectively. To the best of our knowledge, this is the first demonstration of the expression of $GABA_BR$ on NPC SVZ. Then, we demonstrated that taurine increases the number of DCX+ cells, favors neurite outgrowth, and promotes the development of secondary, tertiary, and higher-order neurites. These morphological changes are accompanied by the functional expression of ionic channels mediating inward and outward currents that differentially respond to the activation or blockade of GABA receptors. Since the entire maturation process was sensitive to PTX, it was mediated by the activation of $GABA_AR$ [15]. We also showed that pharmacological activation of $GABA_BR$ in the presence of taurine does not promote neurite outgrowth, neurite development, or functional expression of ion channels.

Contrary to this finding, the blockade of $GABA_BR$ with its specific antagonist CGP 35348 promoted neurite branching and stimulated the development of secondary, tertiary, and higher-order neurites of disaggregated NPC SVZ. We also demonstrated that the taurine interaction with GABA receptors involves an intracellular calcium rise that activates different signaling cascades that stimulate neurite outgrowth. Collectively, these findings show that ionotropic and metabotropic GABA receptors play bidirectional roles in the differentiation and maturation process of NPC SVZ stimulated with taurine.

Role of $GABA_AR$ in the differentiation process of NPC SVZ

The role of GABA in the proliferation, differentiation, and maturation process of NPC SVZ and NPCs of the subgranular zone of the dentate gyrus has been well documented. In both neuronal niches, NPCs express the synthesizing enzyme for GABA, glutamate decarboxylase, several GABA transporters, and, in a spatiotemporal manner, $GABA_AR$ [23, 25, 26]. In the SVZ, GABA is released in a nonsynaptic fashion, and its binding to the $GABA_AR$ triggers depolarization of NPCs [23, 26, 27]. Central to this depolarization process is the inverse chloride gradient during early neuronal development.

It is well documented that the extrusion of intracellular chloride mediated by GABA binding to the $GABA_AR$ leads to membrane depolarization with the subsequent activation of different voltage-sensitive channels [28, 29], including L-type calcium channels [30–32]. A Ca^{2+} influx via L-type channels activates calcium-dependent signaling cascades, including kinases and nuclear factors that control gene expression and cell fate. Consistent with this activity, neurons differentiated from NPCs express the Ca^{2+}–calmodulin-dependent protein kinase II (CaMKII) [33]. Activation of CaMKII phosphorylates the cellular transcription factor, the cAMP response element-binding protein (CREB) that, in turn, controls the transcription of genes critical for neurogenesis, synaptic plasticity, and neuronal survival [34, 35]. We have provided experimental evidence showing that the blockade of CaMKII with KN-93 inhibits neurite outgrowth and neurite branching, suggesting that calcium elevation via $GABA_AR$ activates CaMKII and possibly nuclear CREB.

Consistent with this possibility, CREB promotes the neuronal differentiation of NPCs [36, 37]. Likewise, the taurine-$GABA_AR$ interaction may activate other Ca^{2+}-dependent kinases, including members of the non-receptor Src-family kinases (SFKs), a family of tyrosine kinases that regulate cell growth, differentiation, migration, and survival. Src activation phosphorylates the focal adhesion kinase (FAK) that regulates proliferation and survival via CREB phosphorylation [38]. The plausible participation of the Src kinases, FAK, and CREB in neurite outgrowth was corroborated in our study since the Src inhibitor hindered neurite development of NPC SVZ. In addition, the activation of this signaling cascade is complemented by the possible activation of PIK_3 by Src, which, in turn, activates AKT, a kinase involved in cytoskeletal remodeling [39], a necessary step for dendrite development. Our experimental observations indicate that the activation of $GABA_AR$ with taurine triggers a depolarization that activates calcium-dependent intracellular signaling cascades that favor the development of neurites in NPCs.

$GABA_BR$ in the differentiation process of SVZ NPC

Prior research has largely neglected the contribution of $GABA_BR$ in the differentiation process of NPCs. For example, neocortical embryonic NPCs express the $GABA_BR1$ and $GABA_BR2$ subunits of the $GABA_BR$, and the pharmacological activation of the $GABA_BR$ favors the formation of neocortical-derived neurospheres [17]. Likewise, the proliferation and survival of newly born cells depend on $GABA_BR$ activation, and the blockade of $GABA_BR$ increases adult hippocampal neurogenesis [16]. These observations were further corroborated by Giachino et al. [18], who demonstrated the expression of $GABA_BR$ in hippocampal NPCs and that blockade of $GABA_BR$ increased the neuroblast proliferation and differentiation *in vivo*. These authors suggested that intracellular signaling via $GABA_BR$ inhibits neurogenesis and promotes the quiescence of NPCs [18, 19]. Consistent with these observations, we found immunoreactivity to the $GABA_BR1$ and $GABA_BR2$ subunits in neurospheres derived from the SVZ. Since $GABA_BR$ is a metabotropic receptor, its effects should be ascribed to the dissociation of the G_i or G_o protein into $G_{i\alpha}$, $G_{o\alpha,}$ and $G_{\beta\gamma}$ subunits of the protein G coupled to the $GABA_BR$ complex. The family of $G_{i\alpha/o\alpha}$ proteins, can be grouped in $G_{i\alpha}$, comprising the $G_{i\alpha1}$, $G_{i\alpha2}$, and $G_{i\alpha3}$ subunits, and $G_{o\alpha}$, comprising the $G_{o\alpha1}$ and $G_{o\alpha2}$ splice variants. $G_{\alpha i}$ proteins are recognized for their interaction with G protein-coupled receptors (GPCRs) and to inhibit adenylate cyclase (AC) activation, leading to a decrease in cellular cyclic AMP (cAMP) levels. In such a scenario, after $GABA_BR$ activation, the subunit $G_{i\alpha}$ would inhibit the adenylyl cyclase (AC), thus decreasing the levels of cyclic adenosine 3′-5′-monophosphate (cAMP) and protein kinase A activity and decreasing the phosphorylation level of nuclear CREB [40]. Likewise, the decreased levels of cAMP interfere with the functionality of the cAMP-dependent ERK/MAPK activity, and the downregulation of these kinases also negatively impacts the phosphorylation levels of CREB.

Consequently, it is reasonable to assume that the blockade of $GABA_BR$ with CGP55485 yields a number of positive effects related to neuronal differentiation. First, the inactivation of the $G_{i\alpha}$ subunit may increase the amount of cAMP and PKA activity, which would lead to increased levels of CREB phosphorylation [41, 42]. This same component may activate MAPK, another potential pathway toward CREB phosphorylation [43]. In addition, the blockade of $GABA_BR$ would result in transient intracellular Ca^{2+} elevation, a phenomenon that would lead to CAMKII activation and, subsequently, CREB phosphorylation [44]. These plausible mechanisms reflect the complexity and crosstalk of the signaling cascades mediated by the $GABA_A$- and $GABA_B$- receptors that regulate neuronal differentiation.

It is important to consider that other mechanisms may also be involved in the action of taurine in the differentiation process. For example, taurine regulates glutamate receptors and

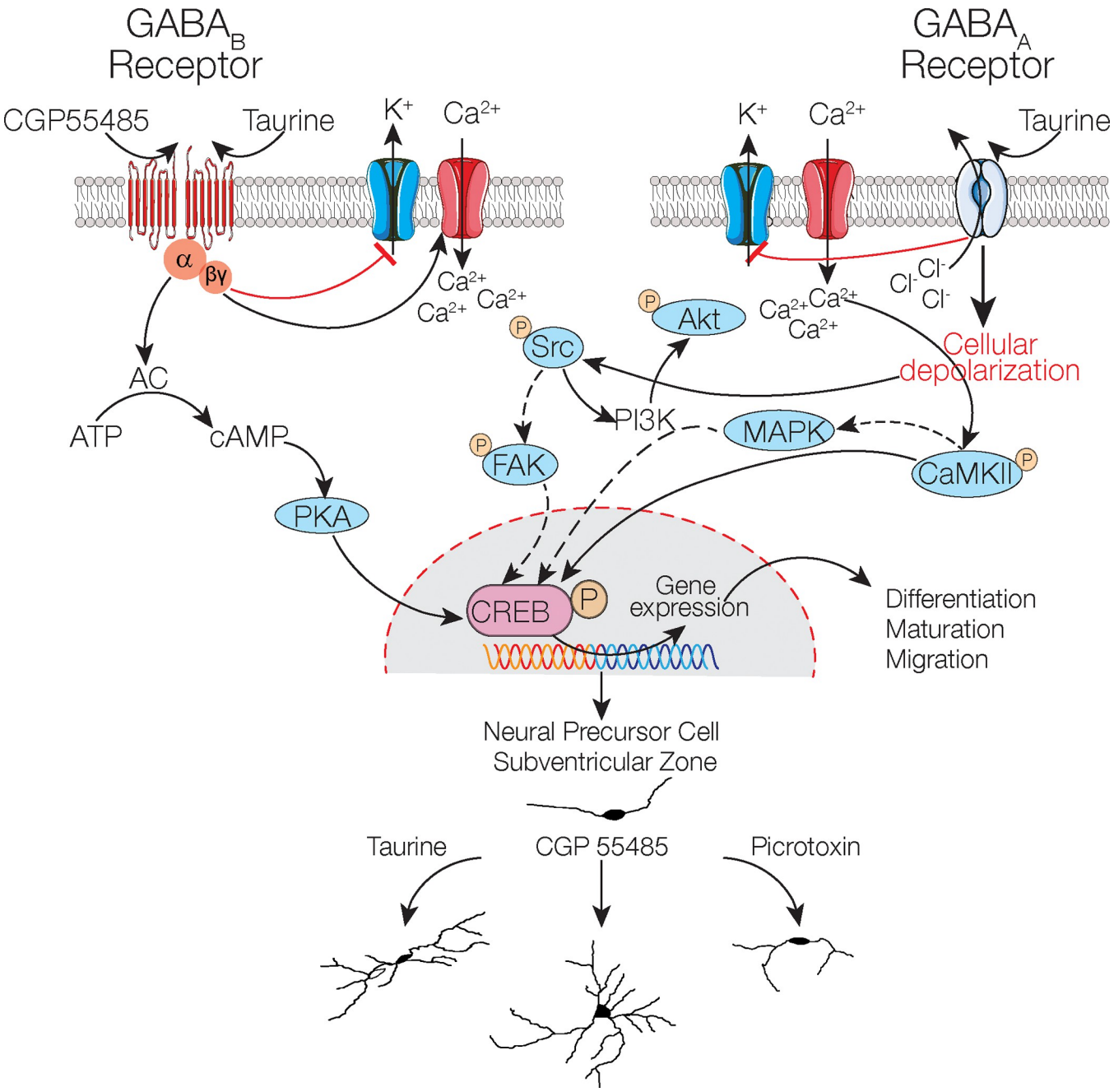

Fig 8. Schematic representation of the possible mechanisms necessary for the differentiation of neural precursor cells of the SVZ mediated by taurine. Taurine binds to the $GABA_A$ receptor and promotes chloride extrusion and the blockade of potassium channels, favoring cellular depolarization, the activation of calcium channels, and activation of the calcium–calmodulin (CaM)–dependent protein kinase II (CaMKII) enzyme that promotes phosphorylation of the cellular transcription factor cAMP response element-binding protein (p-CREB). Cellular depolarization also activates the non-receptor tyrosine kinase Src and phosphorylates protein kinase B or Akt, which is involved in the PI3K/AKT/mTOR signaling cascade. The blockade of the G_i/G_o-linked $GABA_BR$ with CGP55485 may increase the concentration of cAMP, possibly leading to increased CREB phosphorylation via PKA activation or MAPK cascades. Furthermore, its coupling to calcium channels through the $G_{\beta\gamma}$ subunits of the protein G coupled to $GABA_BR$ can allow high intracellular Ca^{2+} levels, activating the CAMKII signaling pathway, thus continuing the pathway mentioned with the $GABA_A$ receptors that could ultimately induce CREB activation.

https://doi.org/10.1371/journal.pone.0305853.g008

modulates intracellular Ca^{2+} signaling, which are essential for regulating neuronal growth and differentiation [45, 46]. These mechanisms may contribute to neuronal differentiation but require additional investigation that was beyond the scope of this study.

Modulation of membranal currents by taurine

Another relevant finding of our study is the selective modulation of membranal currents of NPC SVZ in response to taurine treatments. Although previous studies have documented the acute effect of taurine on the membrane potential, R_N, and action potential firing of immature and mature neurons, these effects are ascribed to an acute-chloride modulation via GABA and glycine receptors [47–51]. This possibility is unlikely in our case because NPC of the SVZ were incubated with taurine for 14 days before any experimental manipulation. One possible explanation for the electrophysiological modulation observed in our study is that taurine, in the long term, favors the adequate assembly of ionic channels rather than acutely modulating chloride conductance to alter the kinetics of the inward and outward currents. We hypothesize that this effect is an additional consequence of the differentiation capacity of taurine; however, this premise requires additional investigation (Fig 8).

Previous studies have demonstrated that the inward current evoked by the protocol used in our study is sensitive to TTX [52], which supports the notion that the taurine-mediated differentiation process of NPC SVZ involves the membranal expression of voltage-gated Na^+ channels responsible for the action potential generation [15]. On the other hand, the kinetics of the outward currents observed in this study resemble the 4-AP-sensitive fast-inactivating K^+ current and the TEA-sensitive delayed K^+ current recorded in actual neurons [22, 24]. Taken together, our results suggest that taurine has the potential to selectively modulate the outward currents that determine the passive properties of excitable cells. Although additional experiments are needed to demonstrate whether taurine has the potential to stimulate the appropriate subunit assembly of ion channels, this study provides evidence that taurine has both morphogenic and electrophysiological properties to control the differentiation and maturation process of neural progenitor cells.

Conclusion

The free amino acid taurine plays a central role in neurite outgrowth and the functional expression of ion channels that determine the passive properties of differentiated cells. Our data show that this effect occurs via GABA receptors and the subsequent activation of signaling cascades expressed by NPC SVZ. Likewise, our data suggest that GABA, acting via the ionotropic or the metabotropic receptors, has opposing effects that control adult neurogenesis in the SVZ.

Acknowledgments

We thank the Faculty of Medicine, UNAM, Dr. Claudia Verónica Rivera Cerecedo, of the Institute of Cell Physiology, UNAM, for the animals used in this study, and Conahcyt fellowship 783563 (NEGC).

Author Contributions

Conceptualization: Nadia Estefanía Gutierrez-Castañeda, Lenin David Ochoa-de la Paz, Emilio J. Galván.

Data curation: Nadia Estefanía Gutierrez-Castañeda, Emilio J. Galván.

Formal analysis: Nadia Estefanía Gutierrez-Castañeda, Vladimir Allex Martínez-Rojas, Emilio J. Galván.

Funding acquisition: Lenin David Ochoa-de la Paz, Emilio J. Galván.

Investigation: Vladimir Allex Martínez-Rojas, Emilio J. Galván.

Methodology: Lenin David Ochoa-de la Paz, Emilio J. Galván.

Project administration: Lenin David Ochoa-de la Paz, Emilio J. Galván.

Resources: Emilio J. Galván.

Validation: Emilio J. Galván.

Writing – original draft: Nadia Estefanía Gutierrez-Castañeda, Vladimir Allex Martínez-Rojas, Emilio J. Galván.

Writing – review & editing: Emilio J. Galván.

References

1. Akers KG, Martinez-Canabal A, Restivo L, Yiu AP, De Cristofaro A, Hsiang HL, et al. Hippocampal neurogenesis regulates forgetting during adulthood and infancy. Science [Internet]. 2014 [cited 2024 Mar 9]; 344(6184):598–602. Available from: https://pubmed.ncbi.nlm.nih.gov/24812394/ https://doi.org/10.1126/science.1248903 PMID: 24812394
2. Altman J, Das GD. Autoradiographic and histological evidence of postnatal hippocampal neurogenesis in rats. J Comp Neurol [Internet]. 1965 [cited 2024 Mar 9]; 124(3):319–35. Available from: https://pubmed.ncbi.nlm.nih.gov/5861717/ https://doi.org/10.1002/cne.901240303 PMID: 5861717
3. Snyder JS, Soumier A, Brewer M, Pickel J, Cameron HA. Adult hippocampal neurogenesis buffers stress responses and depressive behaviour. Nature [Internet]. 2011 Aug 25 [cited 2024 Mar 9]; 476 (7361):458–62. Available from: https://pubmed.ncbi.nlm.nih.gov/21814201/ https://doi.org/10.1038/nature10287 PMID: 21814201
4. Zhao C, Teng EM, Summers RG, Ming GL, Gage FH. Distinct Morphological Stages of Dentate Granule Neuron Maturation in the Adult Mouse Hippocampus. Journal of Neuroscience [Internet]. 2006 Jan 4 [cited 2024 Mar 9]; 26(1):3–11. Available from: https://www.jneurosci.org/content/26/1/3 https://doi.org/10.1523/JNEUROSCI.3648-05.2006 PMID: 16399667
5. Inta D, Alfonso J, Von Engelhardt J, Kreuzberg MM, Meyer AH, Van Hooft JA, et al. Neurogenesis and widespread forebrain migration of distinct GABAergic neurons from the postnatal subventricular zone. Proc Natl Acad Sci U S A [Internet]. 2008 Dec 30 [cited 2024 Mar 9]; 105(52):20994–9. Available from: https://pubmed.ncbi.nlm.nih.gov/19095802/ https://doi.org/10.1073/pnas.0807059105 PMID: 19095802
6. Lois C, Alvarez-Buylla A. Proliferating subventricular zone cells in the adult mammalian forebrain can differentiate into neurons and glia. Proc Natl Acad Sci U S A [Internet]. 1993 Mar 1 [cited 2024 Mar 9]; 90(5):2074–7. Available from: https://pubmed.ncbi.nlm.nih.gov/8446631/ https://doi.org/10.1073/pnas.90.5.2074 PMID: 8446631
7. Alonso M, Lepousez G, Wagner S, Bardy C, Gabellec MM, Torquet N, et al. Activation of adult-born neurons facilitates learning and memory. Nat Neurosci [Internet]. 2012 Jun [cited 2024 Mar 9]; 15 (6):897–904. Available from: https://pubmed.ncbi.nlm.nih.gov/22581183/ https://doi.org/10.1038/nn.3108 PMID: 22581183
8. Sahay A, Wilson DA, Hen R. Pattern separation: a common function for new neurons in hippocampus and olfactory bulb. Neuron [Internet]. 2011 May 26 [cited 2024 Mar 9]; 70(4):582–8. Available from: https://pubmed.ncbi.nlm.nih.gov/21609817/ https://doi.org/10.1016/j.neuron.2011.05.012 PMID: 21609817
9. Zhang Q, Yu Y, Huang XF. Olanzapine Prevents the PCP-induced Reduction in the Neurite Outgrowth of Prefrontal Cortical Neurons via NRG1. Sci Rep [Internet]. 2016 Jan 19 [cited 2024 Mar 9];6. Available from: https://pubmed.ncbi.nlm.nih.gov/26781398/ https://doi.org/10.1038/srep19581 PMID: 26781398
10. Sogawa Y, Yoshimura Y, Otaka A, Yamauchi T. Ca2+-independent activity of Ca2+/calmodulin-dependent protein kinase II involved in stimulation of neurite outgrowth in neuroblastoma cells. Brain Res. 2000 Oct 27; 881(2):165–75. https://doi.org/10.1016/s0006-8993(00)02838-9 PMID: 11036155
11. Gampe K, Brill MS, Momma S, Götz M, Zimmermann H. EGF induces CREB and ERK activation at the wall of the mouse lateral ventricles. Brain Res [Internet]. 2011 Feb 28 [cited 2024 Mar 9]; 1376:31–41.

Available from: https://pubmed.ncbi.nlm.nih.gov/21081118/ https://doi.org/10.1016/j.brainres.2010.11.040 PMID: 21081118

12. Herold S, Jagasia R, Merz K, Wassmer K, Lie DC. CREB signalling regulates early survival, neuronal gene expression and morphological development in adult subventricular zone neurogenesis. Mol Cell Neurosci [Internet]. 2011 Jan [cited 2024 Mar 9]; 46(1):79–88. Available from: https://pubmed.ncbi.nlm.nih.gov/20801218/ https://doi.org/10.1016/j.mcn.2010.08.008 PMID: 20801218

13. Huxtable RJ. Physiological actions of taurine. Physiol Rev [Internet]. 1992 [cited 2024 Mar 17]; 72 (1):101–63. Available from: https://pubmed.ncbi.nlm.nih.gov/1731369/ https://doi.org/10.1152/physrev.1992.72.1.101 PMID: 1731369

14. Mersman B, Zaidi W, Syed NI, Xu F. Taurine Promotes Neurite Outgrowth and Synapse Development of Both Vertebrate and Invertebrate Central Neurons. Front Synaptic Neurosci. 2020 Jul 22; 12:548210. https://doi.org/10.3389/fnsyn.2020.00029 PMID: 32792935

15. Gutiérrez-Castañeda NE, González-Corona J, Griego E, Galván EJ, Ochoa-de la Paz LD. Taurine Promotes Differentiation and Maturation of Neural Stem/Progenitor Cells from the Subventricular Zone via Activation of GABAA Receptors. Neurochem Res [Internet]. 2023 Jul 1 [cited 2024 Mar 9]; 48(7):2206–19. Available from: https://pubmed.ncbi.nlm.nih.gov/36862323/ https://doi.org/10.1007/s11064-023-03883-2 PMID: 36862323

16. Felice D, O'Leary OF, Pizzo RC, Cryan JF. Blockade of the GABA(B) receptor increases neurogenesis in the ventral but not dorsal adult hippocampus: relevance to antidepressant action. Neuropharmacology [Internet]. 2012 Dec [cited 2024 Mar 9]; 63(8):1380–8. Available from: https://pubmed.ncbi.nlm.nih.gov/22884610/ https://doi.org/10.1016/j.neuropharm.2012.06.066 PMID: 22884610

17. Fukui M, Nakamichi N, Yoneyama M, Ozawa S, Fujimori S, Takahata Y, et al. Modulation of cellular proliferation and differentiation through GABA(B) receptors expressed by undifferentiated neural progenitor cells isolated from fetal mouse brain. J Cell Physiol [Internet]. 2008 Aug [cited 2024 Mar 9]; 216(2):507–19. Available from: https://pubmed.ncbi.nlm.nih.gov/18302163/ https://doi.org/10.1002/jcp.21422 PMID: 18302163

18. Giachino C, Barz M, Tchorz JS, Tome M, Gassmann M, Bischofberger J, et al. GABA suppresses neurogenesis in the adult hippocampus through GABAB receptors. Development [Internet]. 2014 Jan 1 [cited 2024 Mar 9]; 141(1):83–90. Available from: https://doi.org/10.1242/dev.102608 PMID: 24284211

19. Gustorff C, Scheuer T, Schmitz T, Bührer C, Endesfelder S. GABAB Receptor-Mediated Impairment of Intermediate Progenitor Maturation During Postnatal Hippocampal Neurogenesis of Newborn Rats. Front Cell Neurosci [Internet]. 2021 Aug 6 [cited 2024 Mar 9]; 15. Available from: https://pubmed.ncbi.nlm.nih.gov/34421540/ https://doi.org/10.3389/fncel.2021.651072 PMID: 34421540

20. Schneider CA, Rasband WS, Eliceiri KW. NIH Image to ImageJ: 25 years of image analysis. Nature Methods 2012 9:7 [Internet]. 2012 Jun 28 [cited 2024 Mar 9]; 9(7):671–5. Available from: https://www.nature.com/articles/nmeth.2089 https://doi.org/10.1038/nmeth.2089 PMID: 22930834

21. Ferreira TA, Blackman A V., Oyrer J, Jayabal S, Chung AJ, Watt AJ, et al. Neuronal morphometry directly from bitmap images. Nature Methods 2014 11:10 [Internet]. 2014 Sep 29 [cited 2024 Mar 9]; 11 (10):982–4. Available from: https://www.nature.com/articles/nmeth.3125 https://doi.org/10.1038/nmeth.3125 PMID: 25264773

22. Griego E, Herrera-López G, Gómez-Lira G, Barrionuevo G, Gutiérrez R, Galván EJ. Functional expression of TrkB receptors on interneurones and pyramidal cells of area CA3 of the rat hippocampus. Neuropharmacology. 2021 Jan 1; 182:108379. https://doi.org/10.1016/j.neuropharm.2020.108379 PMID: 33130041

23. Stewart RR, Hoge GJ, Zigova T, Luskin MB. Neural progenitor cells of the neonatal rat anterior subventricular zone express functional GABAA receptors. J Neurobiol [Internet]. 2002 Mar 1 [cited 2024 Mar 9]; 50(4):305–22. Available from: https://onlinelibrary.wiley.com/doi/full/10.1002/neu.10038 PMID: 11891665

24. Griego E, Segura-Villalobos D, Lamas M, Galván EJ. Maternal immune activation increases excitability via downregulation of A-type potassium channels and reduces dendritic complexity of hippocampal neurons of the offspring. Brain Behav Immun. 2022 Oct 1; 105:67–81. https://doi.org/10.1016/j.bbi.2022.07.005 PMID: 35803480

25. Bordey A. Adult-born neuron development is controlled by GABAA receptor subtypes (Commentary on Duveau et al.). Eur J Neurosci [Internet]. 2011 Aug [cited 2024 Mar 9]; 34(3):361. Available from: https://pubmed.ncbi.nlm.nih.gov/21801241/ https://doi.org/10.1111/j.1460-9568.2011.07807.x PMID: 21801241

26. Liu X, Wang Q, Haydar TF, Bordey A. Nonsynaptic GABA signaling in postnatal subventricular zone controls GFAP-expressing progenitor proliferation. Nat Neurosci [Internet]. 2005 Sep [cited 2024 Mar 9]; 8(9):1179. Available from: /pmc/articles/PMC1380263/

27. Wang J, Liu SH, Haditsch U, Tu WH, Cochrane K, Ahmadian G, et al. Interaction of calcineurin and type-A GABA receptor gamma 2 subunits produces long-term depression at CA1 inhibitory synapses. J Neurosci [Internet]. 2003 Feb 1 [cited 2024 Mar 9]; 23(3):826–36. Available from: https://pubmed.ncbi.nlm.nih.gov/12574411/ https://doi.org/10.1523/JNEUROSCI.23-03-00826.2003 PMID: 12574411

28. Agosti F, Cordisco Gonzalez S, Martinez Damonte V, Tolosa MJ, Di Siervi N, Schioth HB, et al. Melanocortin 4 receptor constitutive activity inhibits L-type voltage-gated calcium channels in neurons. Neuroscience [Internet]. 2017 Mar 27 [cited 2024 Mar 9]; 346:102–12. Available from: https://ri.conicet.gov.ar/handle/11336/40431 https://doi.org/10.1016/j.neuroscience.2017.01.007 PMID: 28093215

29. Toth AB, Shum AK, Prakriya M. Regulation of neurogenesis by calcium signaling. Cell Calcium [Internet]. 2016 Mar 1 [cited 2024 Mar 9]; 59(2–3):124–34. Available from: https://pubmed.ncbi.nlm.nih.gov/27020657/ https://doi.org/10.1016/j.ceca.2016.02.011 PMID: 27020657

30. D'Ascenzo M, Piacentini R, Casalbore P, Budoni M, Pallini R, Azzena GB, et al. Role of L-type Ca2+ channels in neural stem/progenitor cell differentiation. European Journal of Neuroscience [Internet]. 2006 Feb 1 [cited 2024 Mar 9]; 23(4):935–44. Available from: https://onlinelibrary.wiley.com/doi/full/10.1111/j.1460-9568.2006.04628.x PMID: 16519658

31. Loturco JJ, Owens DF, Heath MJS, Davis M 8 E, Kriegsteing AR. GABA and Glutamate Depolarize Cortical Progenitor Cells and Inhibit DNA Synthesis. Neuron. 1287;15. https://doi.org/10.1016/0896-6273(95)90008-x PMID: 8845153

32. Nguyen L, Malgrange B, Breuskin I, Bettendorff L, Moonen G, Belachew S, et al. Autocrine/Paracrine Activation of the GABA A Receptor Inhibits the Proliferation of Neurogenic Polysialylated Neural Cell Adhesion Molecule-Positive (PSA-NCAM) Precursor Cells from Postnatal Striatum. 2003; https://doi.org/10.1523/JNEUROSCI.23-08-03278.2003 PMID: 12716935

33. Kutcher LW, Beauman SR, Gruenstein EI, Kaetzel MA, Dedman JR. Nuclear CaMKII inhibits neuronal differentiation of PC12 cells without affecting MAPK or CREB activation. Am J Physiol Cell Physiol [Internet]. 2003 Jun 1 [cited 2024 Mar 9]; 284(6 53–6):1334–45. Available from: https://journals.physiology.org/doi/10.1152/ajpcell.00510.2002 PMID: 12570987

34. Lonze BE, Ginty DD. Function and regulation of CREB family transcription factors in the nervous system. Neuron [Internet]. 2002 Aug 15 [cited 2024 Mar 9]; 35(4):605–23. Available from: https://pubmed.ncbi.nlm.nih.gov/12194863/ https://doi.org/10.1016/s0896-6273(02)00828-0 PMID: 12194863

35. Yan X, Liu J, Ye Z, Huang J, He F, Xiao W, et al. CaMKII-Mediated CREB Phosphorylation Is Involved in Ca2+-Induced BDNF mRNA Transcription and Neurite Outgrowth Promoted by Electrical Stimulation. PLoS One [Internet]. 2016 Sep 1 [cited 2024 Mar 9]; 11(9):e0162784. Available from: https://journals.plos.org/plosone/article?id=10.1371/journal.pone.0162784 PMID: 27611779

36. Landeira BS, Santana TTDS, Araújo JADM, Tabet EI, Tannous BA, Schroeder T, et al. Activity-Independent Effects of CREB on Neuronal Survival and Differentiation during Mouse Cerebral Cortex Development. Cerebral Cortex [Internet]. 2018 Feb 1 [cited 2024 Mar 10]; 28(2):538–48. Available from: https://dx.doi.org/10.1093/cercor/bhw387 PMID: 27999124

37. Peltier J, O'Neill A, Schaffer D V. PI3K/Akt and CREB regulate adult neural hippocampal progenitor proliferation and differentiation. Dev Neurobiol [Internet]. 2007 Sep 1 [cited 2024 Mar 9]; 67(10):1348–61. Available from: https://onlinelibrary.wiley.com/doi/full/10.1002/dneu.20506 PMID: 17638387

38. Schlaepfer DD, Hunter T. Focal adhesion kinase overexpression enhances ras-dependent integrin signaling to ERK2/mitogen-activated protein kinase through interactions with and activation of c-Src. J Biol Chem [Internet]. 1997 May 16 [cited 2024 Mar 9]; 272(20):13189–95. Available from: https://pubmed.ncbi.nlm.nih.gov/9148935/ https://doi.org/10.1074/jbc.272.20.13189 PMID: 9148935

39. Manning BD, Toker A. AKT/PKB Signaling: Navigating the Network. Cell [Internet]. 2017 Apr 20 [cited 2024 Mar 9]; 169(3):381–405. Available from: https://pubmed.ncbi.nlm.nih.gov/28431241/

40. Ma TC, Barco A, Ratan RR, Willis DE. cAMP-responsive Element-binding Protein (CREB) and cAMP Co-regulate Activator Protein 1 (AP1)-dependent Regeneration-associated Gene Expression and Neurite Growth *. 2014; https://doi.org/10.1074/jbc.M114.582460 PMID: 25296755

41. Lepski G, Jannes CE, Nikkhah G, Bischofberger J. cAMP promotes the differentiation of neural progenitor cells in vitro via modulation of voltage-gated calcium channels. Front Cell Neurosci. 2013 Sep 19; (SEP). https://doi.org/10.3389/fncel.2013.00155 PMID: 24065885

42. Zhang X, Odom DT, Koo SH, Conkright MD, Canettieri G, Best J, et al. Genome-wide analysis of cAMP-response element binding protein occupancy, phosphorylation, and target gene activation in human tissues. Proc Natl Acad Sci U S A [Internet]. 2005 Mar 22 [cited 2024 Mar 9]; 102(12):4459–64. Available from: https://pubmed.ncbi.nlm.nih.gov/15753290/ https://doi.org/10.1073/pnas.0501076102 PMID: 15753290

43. Pearson G, Robinson F, Beers Gibson T, Xu B e, Karandikar M, Berman K, et al. Mitogen-activated protein (MAP) kinase pathways: regulation and physiological functions. Endocr Rev [Internet]. 2001 Apr 1

[cited 2024 Mar 9]; 22(2):153–83. Available from: https://pubmed.ncbi.nlm.nih.gov/11294822/ https://doi.org/10.1210/edrv.22.2.0428 PMID: 11294822

44. Wayman GA, Lee YS, Tokumitsu H, Silva A, Soderling TR. Calmodulin-Kinases: Modulators of Neuronal Development and Plasticity.

45. Wang Q, Zhu GH, Xie DH, Wu WJ, Hu P. Taurine Enhances Excitability of Mouse Cochlear Neural Stem Cells by Selectively Promoting Differentiation of Glutamatergic Neurons Over GABAergic Neurons. Neurochem Res [Internet]. 2015 May 1 [cited 2024 Mar 9]; 40(5):924–31. Available from: https://link.springer.com/article/10.1007/s11064-015-1546-9 PMID: 25725997

46. Yang J, Guo H, Sun D, Duan J, Rao X, Xu F, et al. Elevated glutamate, glutamine and GABA levels and reduced taurine level in a schizophrenia model using an in vitro proton nuclear magnetic resonance method. Am J Transl Res [Internet]. 2019 [cited 2024 Mar 9]; 11(9):5919. Available from: /pmc/articles/PMC6789232/ PMID: 31632560

47. Belluzzi O, Puopolo M, Benedusi M, Kratskin I. Selective neuroinhibitory effects of taurine in slices of rat main olfactory bulb. Neuroscience [Internet]. 2004 [cited 2024 Mar 17]; 124(4):929–44. Available from: https://pubmed.ncbi.nlm.nih.gov/15026133/ https://doi.org/10.1016/j.neuroscience.2003.12.032 PMID: 15026133

48. Furukawa T, Fukuda A. Maternal taurine as a modulator of Cl–homeostasis as well as of glycine/GABAA receptors for neocortical development. Front Cell Neurosci [Internet]. 2023 [cited 2024 Mar 9]; 17:1221441. Available from: /pmc/articles/PMC10435090/

49. Hosoi Y, Akita T, Watanabe M, Ito T, Miyajima H, Fukuda A. Taurine depletion during fetal and postnatal development blunts firing responses of neocortical layer II/III pyramidal neurons. Front Mol Neurosci. 2022 Nov 17; 15:806798. https://doi.org/10.3389/fnmol.2022.806798 PMID: 36466806

50. Jiang Z, Krnjević K, Wang F, Ye JH. Taurine Activates Strychnine-Sensitive Glycine Receptors in Neurons Freshly Isolated from Nucleus Accumbens of Young Rats. J Neurophysiol [Internet]. 2004 Jan [cited 2024 Mar 17]; 91(1):248–57. Available from: https://journals.physiology.org/doi/10.1152/jn.00106.2003 PMID: 12878709

51. Sava BA, Chen R, Sun H, Luhmann HJ, Kilb W. Taurine activates GABAergic networks in the neocortex of immature mice. Front Cell Neurosci. 2014 Feb 4; 8(FEB):69584. https://doi.org/10.3389/fncel.2014.00026 PMID: 24550782

52. Martínez-Rojas VA, Arosio D, Pennuto M, Musio C. Clenbuterol-sensitive delayed outward potassium currents in a cell model of spinal and bulbar muscular atrophy. Pflugers Arch [Internet]. 2021 Aug 1 [cited 2024 Mar 9]; 473(8):1213–27. Available from: https://pubmed.ncbi.nlm.nih.gov/34021780/ https://doi.org/10.1007/s00424-021-02559-6 PMID: 34021780